2011

Rotate and Hold and Scan (RAHAS): Structured Light Illumination for Use in Remote Areas

Eli Ross Crane
University of Kentucky, eli.crane@engr.uky.edu

ABSTRACT OF THESIS

Rotate and Hold and Scan (RAHAS):
Structured Light Illumination for Use in Remote Areas.

As a critical step after the discovery of material culture in the field, archaeologists have a need to document these findings with a slew of different physical measurements and photographs from varying perspectives. 3-D imaging is becoming increasingly popular as the primary documenting method to replace the plethora of tests and measurements, but for remote areas 3-D becomes more cumbersome due to physical and environmental constraints. The difficulty of using a 3-D imaging system in such environments is drastically lessened while using the RAHAS technique, since it acquires scans untethered to a computer. The goal of this thesis is to present the RAHAS Structured Light Illumination technique for 3-D image acquisition, and the performance of the RAHAS technique as a measurement tool for documentation of material culture on a field trip to the Rio Platano Biosphere in Honduras.

KEYWORDS: Structured Light Illumination, 3-D Scanner, Remote, In situ

Eli R Crane

March 20, 2011

Rotate and Hold and Scan (RAHAS): Structured Light Illumination for Use in Remote Areas.

By

Eli Ross Crane

Dr. Laurence G. Hassebrook
Director of Thesis

Dr. Stephen Gedney
Director of Graduate Studies

March 20, 2011

RULES FOR THE USE OF THESES

Unpublished theses submitted for the Master's degree and deposited in the University of Kentucky Library are as a rule open for inspection, but are to be used only with due regard to the rights of the authors. Bibliographical references may be noted, but quotations or summaries of parts may be published only with the permission of the author, and with the usual scholarly acknowledgments.

Extensive copying or publication of the thesis in whole or in part also requires the consent of the Dean of the Graduate School of the University of Kentucky.

A library that borrows this thesis for use by its patrons is expected to secure the signature of each user.

Name	Date

THESIS

Eli Ross Crane

The Graduate School

University of Kentucky

2011

Rotate and Hold and Scan (RAHAS): Structured Light Illumination for Use in Remote Areas.

THESIS

A thesis submitted in partial fulfillment of the
requirements for the degree of Master of Science in the
College of Engineering
at the University of Kentucky

By

Eli Ross Crane

Lexington, Kentucky

Director: Dr. Laurence G. Hassebrook, Professor of Electrical Engineering

Lexington, Kentucky

2011

DEDICATION

To my family, friends and teachers.

ACKNOWLEDGEMENTS

Without the help of others, many things would not be possible. As such, there are many people that I owe a debt of gratitude in this culmination of academic achievements thus far in my life. I have been fortunate to come in contact with many people who have shown me great kindness, and who have opened up many unforeseen possibilities.

I would like to offer my deepest thanks to Dr. Hassebrook, who has been my mentor and friend. Not only has he directed my thesis work, but also he has patiently educated me and enthusiastically guided me through much of my academic career. He has helped me to become a better engineer, researcher, and person.

From my first circuits class to now, Dr. Donohue has been another mentor to me that I am thankful. He has always been the teacher that drove me to want to ace his exams, and that would entertain the briefest of indulgences with bizarre audio topics.

While working under Dr. Lau, I worked on an incredible research project, which ultimately led to graduate school. I would like to thank him for being able to teach me even when I do not know what I need to learn, and for the stepping stone opportunity that he offered me years ago.

My friend Dr. Chris Begley, while I have never set foot in a classroom with him, has still taught me much. I would like to thank him for being the catalyst that forced open the natural world for my research, and being my friend and guide on some crazy adventures.

Soon to be Ph.D., Charles Casey has always offered helpful suggestions and participated in brainstorming sessions that invariably last well beyond what is practical. I would like to thank him for providing immense help and for miraculously always understanding all the problems that I posed to him.

As awesome a friend as could be, Weston Johnson has been forthcoming with advice and counseling. I would like to thank him for helping me to find the motivation to continue and succeed. I would also like to thank Dr. Dieter, whom I greatly respect and admire, for teaching me much while outside a classroom setting.

My family and friends remain loving and supportive, forever helping me to realize my potential. I am grateful for my family and friends.

Table of Contents

List of Figures

Chapter 1
Introduction

Section 1.1 Need for Measurement

Since the beginning of recorded history, the need to measure has existed. In the story of Noah's ark, the ark was described as being built in lengths and widths of "cubits." Gold was once measured in shekels [1], and time was, and even continues to be, measured in terms of the sun and the moon. According to the Greek philosopher Protagoras, "Man is the measure of all things," and for thousands of years, measurement standards were in fact that--comparisons to human appendages: the thumb, the fingers, the hand, the foot and even the stride. As populations grew and scientific pursuits evolved, so did the need for standard measures, a common mathematical language, and the development of tools and techniques to capture and understand information needed for scientific inquiry. Scientific investigation is based on the collection, the measurement and the testing of empirical data, and as such, the availability and choice of tools and techniques used has a direct impact on the conclusions drawn from scientific exploration.

Around 6000 B.C.E., famine and other needs to ration food supplies led to one of the first systems of measurement organized for the dissemination of "available stock" for both military and civilian populations [2]. In the second millennium B.C.E., the Egyptians and Babylonians used a common mathematical idea that we now know as the Pythagorean Theorem to measure and generate right angles in construction [3]. This simple device utilized the Pythagorean Triple 3-4-5, and the marking of a piece of string into twelve equally spaced segments. When a measurement was desired the string would be pulled taut into the shape of a right triangle with sides of the 3-4-5 triple and positioned to

measure as desired. The idea that this device was based on evolved into a foundational theorem for both trigonometry and geometry, and inspired the development of many devices used to enhance scientific inquiry.

One such device was invented in 1630 by ChristophScheiner called a pantograph and was documented in "Pantographice" a year later [4]. A pantograph is a mechanical linkage that utilizes a geometric relationship, in the shape of a parallelogram, to transmit and magnify the motion of a probe to a drawing apparatus [5, 6]. While the pantograph was not used for measurement directly, it did increase the viewing capability of minute details through the scaling that it performed.

A modern spin on the pantograph and probably the first three-dimensional measurement device, the Coordinate Measuring Machine (CMM) [7], was invented and widely adopted in manufacturing quality inspection in the early 1960's. The CMM required a stylus/probe to contact the object to trace along its surface similar to how the pantograph's probe traced a path; however, the result was given in (x, y, z) coordinates instead of a scaled copy of the path. Advancement in optical sensors which use laser, CCD and CMOS sensing mechanisms allowed the CMM to detect the surface differences without direct contact with the surface [8]. However, with the invention of these same technologies came the emergence of digital photography and digital light projection devices that brought with them the capabilities for new non-contact three-dimensional measuring systems. Three-dimensional (3-D) data acquisition is a "modern" approach to measuring systems.

Section 1.2 Measurement in Archaeology

Archaeological projects begin in the field with the search and discovery of artifacts or other objects that were left behind by a past culture or people. The archaeological sites where the material culture is found can be anywhere from a planned construction site in an urban area to a dried up riverbed in a rain forest a day's journey from the nearest

settlement. The collection, measurement and analysis of the material culture and the environmental data are key to learning about the past of peoples and their cultures. However, the process of collecting, measuring and analyzing data can be challenging, and the information gained dependent on the tools used in the process. While photographs are currently the primary method of documenting the collected data for field study of artifacts in situ, with measurement of these artifacts performed by hand separately, three-dimensional imaging would improve the scope of knowledge by providing an x, y, and z coordinate for every pixel that can be used for accurate measurement. However, it is not that simple. Depending on the location of the site, the availability and/or accessibility of the equipment and/or resources required, 3-D imaging can be extremely challenging. For example, remote sites often have no power sources and do not easily lend themselves to bringing in equipment to generate it.

In the summer of 2007, a team of 20 scientists travelling in all-terrain vehicles crossed 600 miles of Mongolian steppe to collect 3-D images of 3,000-year-old carved megaliths that had been virtually un-documented [9]. Each of the vehicles carried more than a ton of weight that included power generators, computers, 3-D scanners and other equipment necessary to complete the expedition. The trip was "exhausting", hard on both people and equipment, but the location was at least accessible by vehicle. In contrast, two years later in 2009, our team set out to do a similar task--to gather 3-D images of undocumented petro glyphs in the jungles of Honduras. The jungle environment precluded the use of any type of vehicle. All equipment used at the site had to be carried in by team members or pack animals. The animals carried the majority of the gear to the river where whitewater rafts were loaded to navigate rapids that would bring the team closer to the sites. Besides food and other expedition supplies, only a single 50 lb. Pelican case containing the battery powered 3-D scanner was transported. In other words, the lack of accessibility limited the amount of weight and thus equipment that could be used. Critical to the success of the expedition was the use of a small portable 3-D scanner.

Despite the difficulties of accessing these remote sites, both expeditions set out to gather 3-D imagery of archaeological materials and both used structured light illumination (SLI)

to generate the depth information for the 3-D data. However, the specific SLI techniques differed, allowing the technique used in the 3-D scanner for the Honduras expedition to shed the extra weight of power generators, computers and digital projectors. It is this new portable SLI technology that is the topic of this thesis.

Section 1.3 Structured Light Illumination Historical Perspective

Structured Light Illumination (SLI) is becoming the most widely used active vision [12] method for non-contact three-dimensional (3-D) measurement, applied in the fields of biomedical topology [13], industrial quality control [14, 15], archaeologicaldocumentation [9], biometrics [16], and the entertainment industry. The numerous uses of SLI have lead to an abundance of different methods for the generation of surface topology, although each technique utilizes the basic premise of measuring the specific deformation of a projected light pattern on the surface contours of a target object[17]. The light pattern can take various forms: a spot [12], a single light stripe [17, 18], multiple light stripes[19], a grid[20,21], sine-wave encoded stripes[22], binary encoded stripes, and various other patterns [12].

The way a pattern is utilized to generate 3-D information can vary as well, evolving from the classic SLI approach utilizing a single light stripe. In this classic approach, a single laser stripe is scanned laterally across a surface and a 2-D image is captured for each of the points that the stripe intersects. This causes the 3-D resolution to be directly related to the number if images captured, and drives the inherent costs of processing the data very high. Improved methods utilizing multiple stripes [19] can capitalize on illuminating the entire surfacein the captured image to gain increased performance,butthese multi-striped patterns introduce ambiguities near discontinuities in the target surface, and can be sensitive to the albedo of the surface. Using multi-frame pattern techniques in a sequence, each pixel of the image can be encoded to eliminate the reconstruction ambiguities and sensitivity to the albedo surface. The sequences can consist of color-encoding patterns [23] or binary-encoding patterns [27, 28], but the

multi-frame pattern sequence called phase-measuring Profilometry (PMP) [29]is particularly robust and the focus of this Thesis.

PMP encodes the surface points with specific phase values, with increasing depth resolution when using higher frequency patterns. The downside is that ambiguous reconstruction occurs with higher frequencies, which leads to multiple-frequency PMP techniques [30-32] to resolve the ambiguities with the phase.Using a conventional PMP method, erroneous motion of the target surface causes reconstruction artifacts that are unresolvable; however, a method called Lock and Hold [40, 41]allows thecapture of full 3-D motion with the depth-resolution of a high frequency PMP pattern.

As an evolution of Lock and Hold, the proposed technique of this Thesis,Rotate and Hold and Scan (RAHAS),also utilizes stripe-tracking algorithms to assist in the unambiguous surface reconstruction of a high-frequency PMP scan. While the other SLI techniques discussed above require a computer for controlling a digital projector to generate the sequence of patterns, RAHAS uses a simple slide projector. Without a tethered computer and with the ability to process at a later time, RAHAS is more portable and can be used in a variety of environments.

Section 1.4Thesis Overview

The purpose of this thesis is to outline and present the new SLI process used for generating the 3-D information from the data collected in the Rio Platano Biosphere of Honduras in the summer of 2009.The thesis is organized into five chapters. The first chapter serves as an introduction and gives a brief history of measurement and how measurement pertains to the archaeology field. Chapter 2 contains an overview of different methods for 3-D image capture and a mathematical presentation of phase-measuring profilometry (PMP). The Rotate And Hold And Scan (RAHAS) concept and algorithm are detailed in Chapter 3, along with requirements for a hardware system. The fourth chapter recounts the data collection process in Honduras, shows the 3-D scanner

prototype used, and presents the 3-D image data that was generated using RAHAS. In Chapter 5, final conclusions are made pertaining to the performance of the whole RAHAS process and possible avenues for future work are outlined. Following the chapters of the thesis, there is a glossary with pertinent RAHAS terms and an Appendix containing information that is not part of the main idea of the thesis, but pertains to a broader understanding of the topic.

Chapter 2
Background

The purpose of this chapter is to acclimate the reader with various 3-D acquisition techniques, and present a foundation of knowledge focused on Structured Light Illumination and Phase Measuring Profilometry. The chapter begins with the concept of triangulation as the basis of optical system 3-D reconstruction, then gives an overview of different 3-D acquisition techniques and briefly presents their benefits or drawbacks. Both passive and active acquisition techniques are mentioned, leading to the discussion of Structured Light Illumination and Phase-Measuring Profilometry as the focus of this thesis. The last section discusses the calibration and 3-D reconstruction methods used in this thesis.

Section 2.1 Overview of Three-Dimensional Techniques

Three-dimensional optical measuring techniques can be either passive or active systems. While there are differences between passive or active systems, which will be discussed below, they are all based on using trigonometric relationships between determinable distances and angles to solve for points in the 3-D space. Triangulation is the mathematical determination of a point's position in space using a fixed edge as a known side to a triangle, and the angles between the known side and the lines traced from the end points to the point in space. With the knowledge of a side and two angles of a triangle the other two sides and remaining angle can be calculated.

2.1.1 Passive Optical 3-D Scanner Methods

Passive systems capture depth information from the target amid the current scene with the available ambient light. The passive 3-D acquisition methods that will be discussed

are stereoscopic and photogrammetric. Both utilize cameras to capture two or more images

Stereovision

A basic stereoscopic system would employ two cameras in a known fixed relationship, and use the difference in position of a projected point on the two camera's image planes to triangulate the depth of this point in 3-D space [10]. While stereoscopic imaging is simple and widely used, spanning the fields of biology, engineering and entertainment, the correspondence of points between the two images still poses a problem. Finding the corresponding point for every point in an image is a difficult task, which limits the accuracy that can be achieved by the stereoscopic method.

Photogrammetry

In photogrammetric 3-D acquisition methods a single camera is utilized to capture multiple images from various viewing angles of the target scene [11]. The main issue is that the position and orientation of the camera for each image has to be determined. This process is called resection, and is performed by solving a system of geometric relationships that are determined by finding correspondences between all images. The correspondences of each image are usedto trace intersecting lines back to each camera forming the system of geometric relationships. Depth is then generated from triangulation after resection. Again, finding the same point in each image is not a simple task.

2.1.2 Active optical 3-D Scanner Methods

In an active optical 3-D scanner system, light is introduced to the scene while a camera or other optical sensor observes. The light can be in the form of temporal laser pulses that allow measurement of distance, one point at a time (the Time of Flight system), or a white or colored light pattern that has the capability for multiple point measurement at a time (Structured Light Illumination).

Time of Flight

At the basis of a Time-of-Flight 3-D scanner is a laser rangefinder that uses the round-trip time between the emission and the detection of a pulsed laser to measure distance to a point on a surface. The distance, d, is calculated using the equation

$$d = \frac{ct}{2} \tag{2.1}$$

where$t$ is the round-trip time and c is the speed of light. Since the laser can only be in contact with a single point at a time, the scanner must trace the surface of the target point by point, while the camera captures the scene within its field-of-view. The 3-D point coordinates are measured using trilateration, which involves using the edge lengths on a triangle to determine coordinate position instead of the use of angles as in triangulation.

Structured Light Illumination (SLI)

Structured light illumination (SLI) is an acquisition technique for digitizing three-dimensional surfaces that has become commonly used in many industries including biometrics, manufacturing, archaeology, etc... SLI works by measuring the specific deformation of a projected light pattern on the surface contours of an object [17]. The pattern is used to identify the points in camera coordinates, so that triangulation can be performed to find the position of each point in 3-D space. There are a variety of pattern types that can be used: single dimensioned lines, two dimensioned stripes, grids or dot matrices. The innovation presented in this paper is a specific application of SLI and will be further detailed in the next chapter.

While a splayed laser beam can be used to project a stripe on the target, a digital projector can remove the need for a mechanical assembly to "scan" or move the stripe along the surface. A digital projector, whether DLP or LCD, projects a 2-D array of pixels on to a target that result in a single pixel corresponding to a specific location on the surface. The depth associated with each pixel in the camera is determined by triangulation of the projected pattern at each pixel with the camera and the projector after a calibration process is performed that defines unknown triangulation parameters.

The need to identify each pixel explicitly has led to many different temporal and spatial techniques for pattern creation for point discrimination, such as Binary or Gray Scale encoding or Phase Measuring Profilometry (PMP). Binary/Gray Scale encodingand PMP employ multiple pattern projections that are time multiplexed, which means that the patterns occur in succession, one after each other. Performing the patterns in succession increases the time to scan for each new pattern that must be included. To save on scanning time and allow real-time processing, the time sequenced pattern can be projected as a single pattern through a technique called *composite pattern*[24-26].

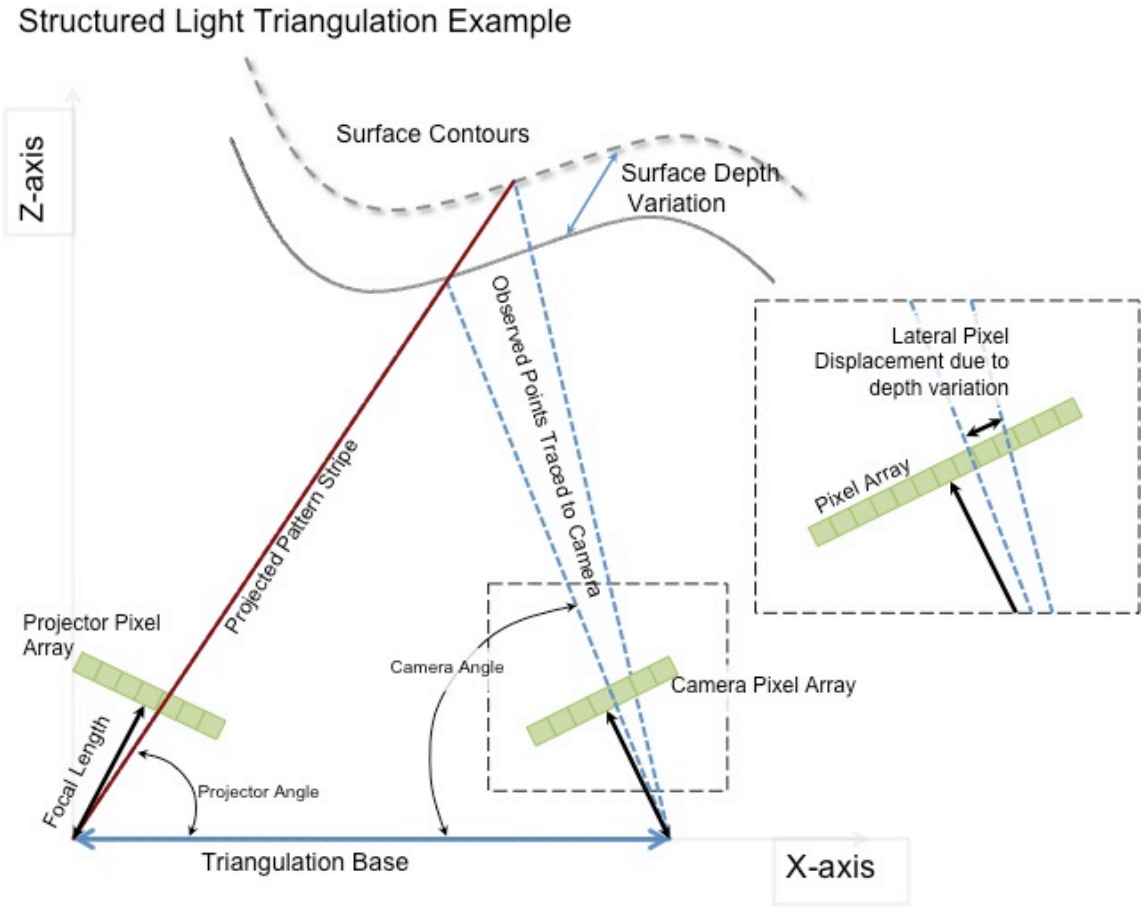

Figure 2.1 Diagram of triangulation in SLI.

With Binary [27]and gray scale[28] encoding a succession of patterns is projected onto the target that encode each pixel with a unique binary code, with each bit corresponding to a single frame in the time-sequence. The main difference between binary and grayscale is that in grayscalethe adjacent regions in the image differ by only a single bit,

which results in an improvement in signal-to-noise ratio. PMP is a robust method and will be discussed in detail in the next section.

Section 2.2 Phase Measuring Profilometry (PMP)

Phase Measuring Profilometry (PMP) [29] as mentioned in the previous section is a method of Structured Light Illumination that measures depth information from a surface using a sequence of phase shifted sinusoidally varying patterns. Much like how Binary Encoding uses a code sequence to identify pixels, a PMP pattern sequence can be thought of as encoding rows in the camera image with values that correspond to the phase shift of a sinusoid. The sequence of projected patterns generate a temporal signal at each pixel, such that the signal is a sinusoid, and the phase of the sinusoid is directly related to the position of the pixel along the Phase Direction. The pattern from the perspective of the projector can be described by the following equation

$$I_n(x^p, y^p) = A^p + B^p \cos\left(2\pi f y^p - \frac{2\pi n}{N}\right) \tag{2.2}$$

where A^p and B^p are constants. The p superscripts denote the projector coordinates. The f is the frequency of the sine pattern measured in cycles per image-frame, N is the total number of phase shifts for the whole sequence, and n is the current phase shift index or current frame in the time sequence. Since the equation depends only on y^p, the intensity value of a given pixel, $I_n(x^p, y^p)$, varies only in the y^p direction. This direction is called the Phase Direction of the PMP pattern because it is the direction of the phase shift. The term Orthogonal Direction is appropriately named for the relationship with the phase direction -- it lies 90 degrees from the Phase Direction along the constant x^p values of the pattern. Figure 2.2shows examples of PMP patterns at three separate frequencies, along with corresponding Phase and Orthogonal Directions.

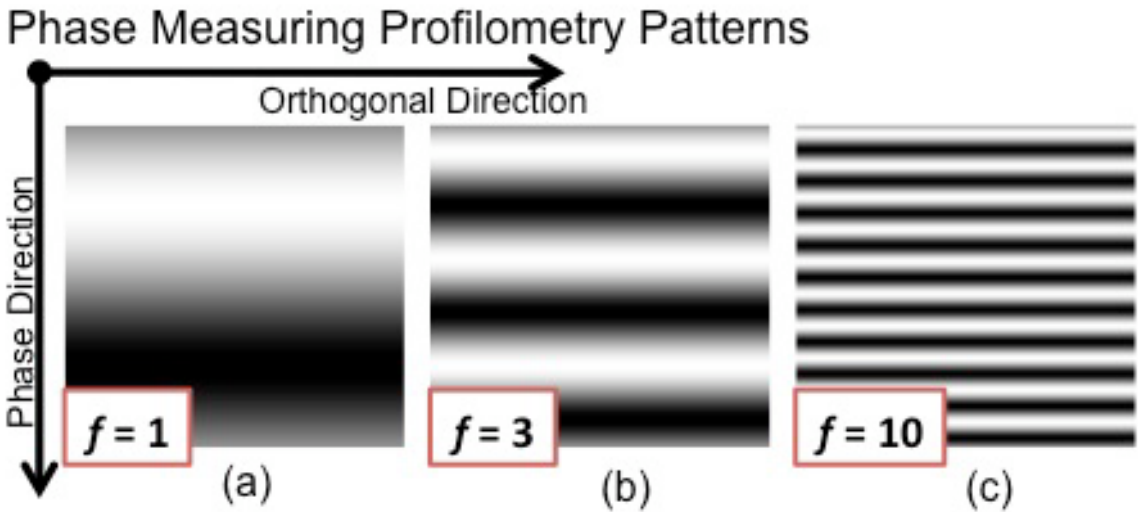

Figure 2.2 Sinusoidal PMP patterns. (a) is at a frequency of 1, (b) is at a frequency of 3 and (c) is at a frequency of 10. A visual description of the terms Phase Direction and Orthogonal Direction are shown with the corresponding relationship to the patterns.

In order to triangulate to a specific point, the point's position in both camera and projector space must be known. While the camera position is known explicitly due to captured image being in camera space, the projector points are determined by matching a phase value measured at a point to that same phase value in the sinusoidally varying pattern as described in Equation 2.2. The phase value at each pixel in the camera space, $\phi(x^c, y^c)$, is determined by projecting *N* phase shifted patterns at the target and processing a sequence of *N* images by the equation

$$\phi(x^c, x^c) = \arctan\left[\frac{\sum_{n=1}^{N} I_n(x^c, y^c)\sin(2\pi n/N)}{\sum_{n=1}^{N} I_n(x^c, y^c)\cos(2\pi n/N)}\right] \tag{2.3}$$

where$n$ denotes an index into the image sequence and $I_n(x^c, y^c)$ is the pixel intensity value at the position (x^c, y^c) in the n^{th} image in the sequence.

For a pattern frequency of 1, which we will call the base frequency or a pattern of a single period of sinusoidal variation, the phase, ϕ, is easily mapped to a projector frame percentage along the Phase Direction by the equation

$$y^p = \frac{\phi(x^c, y^c)}{2\pi f} \tag{2.4}$$

Notice that y^p is not actually a coordinate in the projector space, but it is a value ranging from 0 to 1 that denotes a percentage of the distance between the bottom of the projector frame and the top.

An ambiguous phase problem occurs when increasing the frequency beyond 1 even though better depth resolution can be achieved through the use of higher frequency patterns [30, 33]. The problem is due to the periodic nature in sinusoids, and can be explained by examining the phase variation in $\phi(x^c, y^c)$ and comparing it to Equation 2.4. The variation in $\phi(x^c, y^c)$ is always from 0 to 2π but at $f > 1$Equation 2.4 will only vary between 0 and 1/f. So at higher frequencies, this creates what is called a repeated or Wrapped Phase image that requires unwrapping to fully acquire the unambiguous phase value for the correct y^p coordinate.

To take advantage of the benefits of higher frequency patterns on depth measurement, a technique called multi-frequency PMP [32] was developed that uses lower frequency PMP scans to "unwrap" the phase for the higher frequencies, which allows for better accuracy with fewer number of frames.

Section 2.3 SLI Calibration and Reconstruction

In the previous section, various concepts utilizing triangulation to achieve depth in 3-D surfaces were presented. Triangulation is based upon known geometric relationships to determine the points in a spatial coordinate system; therefore, it is important to the performance of any of these systems that the required geometric parameters be computed in a calibration process [35]. In this section, both the calibration procedure and the reconstruction method used in this thesis are presented.

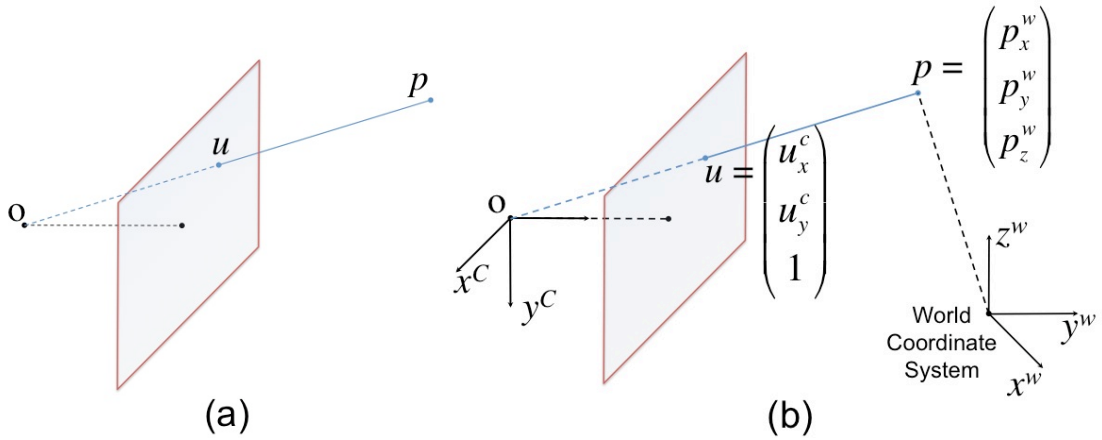

Figure 2.3 The pinhole camera model. (a) shows the ideal pinhole model of the perspective projection of point p onto the image plane as point u, while (b) includes both the Camera and World coordinate systems.

2.3.1 Overview of the model and Triangulation

At the beginning of this chapter, Figure 2.1 used a simple model to visualize triangulation, and although it was not discussed the simplistic pinhole model represented both the camera and projector. Shown in Figure 2.3a, the ideal pinhole model is comprised of a single point *o* called the *center of projection*, and a plane termed the *image plane*. When a line is traced from a point in the 3-D world space to the *center of projection* the line intersects the *image plane* at a single point, which is u in Figure 2.3a. The mapping of the point p in the 3-D coordinate system to the intersected point, u, on the 2-D *image plane*is called the perspective projection and is described by the equation

$$\lambda \begin{pmatrix} u_x \\ u_y \\ 1 \end{pmatrix} = \begin{pmatrix} p_x \\ p_y \\ p_z \end{pmatrix} \tag{2.5}$$

where the *center of projection* is located on the origin of the world coordinate system for the ideal model and λ is a non-zero scalar.

The camera coordinate system and world coordinate system are both represented in Figure 2.3b. The 3-D point p has world coordinates described by the vector $p^w = \left(p_x^w, p_y^w, p_z^w\right)^T$ and camera coordinates described by the vector $p^c = \left(p_x^c, p_y^c, p_z^c\right)^T$. These two vectors are related by the affine transformation specified by the rotation matrix

$R \in \mathbb{R}^{3\times3}$ and the translation vector $T \in \mathbb{R}^3$, such that

$$p^c = Rp^w + T \tag{2.6}$$

The Equation 2.6 can be rewritten and combined with Equation 2.5 as

$$\lambda u = [R|T]\begin{bmatrix}p^w\\1\end{bmatrix} \tag{2.7}$$

Together (R, T) make up the extrinsic parameters [34] of the camera by describing its orientation and location with respect to the world coordinate system. While the extrinsic parameters map the point p^w to p^c, the intrinsic parameters map the point p^c to the 2-D pixel image plane. To compensate for intrinsic parameters such as scaling differences between the image plane and the pixel coordinates, variations in focal length, or a skewed image plane from its actual orientation, a matrix $K \in \mathbb{R}^{3\times3}$ is introduced to the transformation such that

$$\lambda u = K[R|T]\begin{bmatrix}p^w\\1\end{bmatrix} \tag{2.8}$$

which can be further simplified to

$$\lambda u = M\begin{bmatrix}p^w\\1\end{bmatrix} \tag{2.9}$$

where

$$M = \begin{bmatrix}m_1 & m_2 & m_3 & m_4\\ m_5 & m_6 & m_7 & m_8\\ m_9 & m_{10} & m_{11} & m_{12}\end{bmatrix} \tag{2.10}$$

It can be shown [34, 35] that the world to pixel coordinate transforms for a pinhole model follows directly from Equation 2.9, which are

$$x_{c,n} = \frac{m_1 x_{w,n} + m_2 y_{w,n} + m_3 z_{w,n} + m_4}{m_9 x_{w,n} + m_{10} y_{w,n} + m_{11} z_{w,n} + m_{12}} \tag{2.11}$$

and

$$y_{c,n} = \frac{m_5 x_{w,n} + m_6 y_{w,n} + m_7 z_{w,n} + m_8}{m_9 x_{w,n} + m_{10} y_{w,n} + m_{11} z_{w,n} + m_{12}} \tag{2.12}$$

where$n = 1, 2, \ldots, N$ points on a calibration target. These equations assume that the m_{12} term is 1, so that the transformation is linear at the world origin. The calibration procedure generates an image of a calibration target with *N* points on the surface that have known values for $(X_n^w, Y_n^w, Z_n^w, x_n^c, y_n^c)$ for each point on the target. Using this calibration procedure all the terms of the matrix *M* can be determined. It follows that both the matrix M^c for the camera coordinate system and the matrix M^p that represents the projector coordinate transformations are determined using the same method and can be found simultaneously.

2.3.2 The 3-D Reconstruction

A benefit of performing PMP in only the y^p direction is that the equations become simpler, and only three parameters (x^c, y^c, y^p) are necessary for triangulating the corresponding world coordinate for each pixel. Of the required parameters, the camera coordinates (x^c, y^c) are known explicitly, while the y^p value is determined by the specific method for Structured Light Illumination. In this thesis, the y^p values are obtained from the unwrapped phase and the Equation 2.3. To obtain the world coordinate (X^w, Y^w, Z^w), it has been shown [36] that manipulation of Equations 2.11 and 2.12 leads to

$$\begin{bmatrix} m_1 - m_9 x^c & m_2 - m_{10} x^c & m_3 - m_{11} x^c \\ m_5 - m_9 y^c & m_6 - m_{10} y^c & m_7 - m_{11} y^c \\ m_5^p - m_9^p y^p & m_6^p - m_{10}^p y^p & m_7^p - m_{11}^p y^p \end{bmatrix} \begin{bmatrix} X^w \\ Y^w \\ Z^w \end{bmatrix} = \begin{bmatrix} m_{12} x^c - m_4 \\ m_{12} y^c - m_8 \\ m_{12}^p y^p - m_8^p \end{bmatrix} \tag{2.13}$$

and let

$$C = \begin{bmatrix} m_1 - m_9 x^c & m_2 - m_{10} x^c & m_3 - m_{11} x^c \\ m_5 - m_9 y^c & m_6 - m_{10} y^c & m_7 - m_{11} y^c \\ m_5^p - m_9^p y^p & m_6^p - m_{10}^p y^p & m_7^p - m_{11}^p y^p \end{bmatrix} \tag{2.14}$$

$$D = \begin{bmatrix} m_{12} x^c - m_4 \\ m_{12} y^c - m_8 \\ m_{12}^p y^p - m_8^p \end{bmatrix} \tag{2.15}$$

Now back substituting C and D into Equation 2.13, the equation becomes

$$C \begin{bmatrix} X^w \\ Y^w \\ Z^w \end{bmatrix} = D \tag{2.16}$$

and the world coordinate 3-D point can be obtained with

$$\begin{bmatrix} X^w \\ Y^w \\ Z^w \end{bmatrix} = C^{-1} D \tag{2.17}$$

2.3.3 Calibration Process Summary

The first step for calibration is to make a target that has *N* points with measured world coordinates. The calibration grid (shown in Figure 2.4) that was used for all the scans in this thesis was a "roof" shaped grid with *N* = 18 circular marks, 9 in a 3 by 3 array on each slope of the roof. Each mark's (X_n^w, Y_n^w, Z_n^w) coordinate was measured in millimeters relative to the first mark. The next step is to acquire a SLI scan of the calibration target along with the corresponding phase map and y^p values. Using the *N* known points on the surface and the determinedy^p data, the M_n^c and M_n^p matrix values can be calculated completing the calibration procedure. The detailed calibration process used for this thesis, as well as the software used to calibrate the system is outlined and well documented as part of the imaging research group at the University of Kentucky [39].

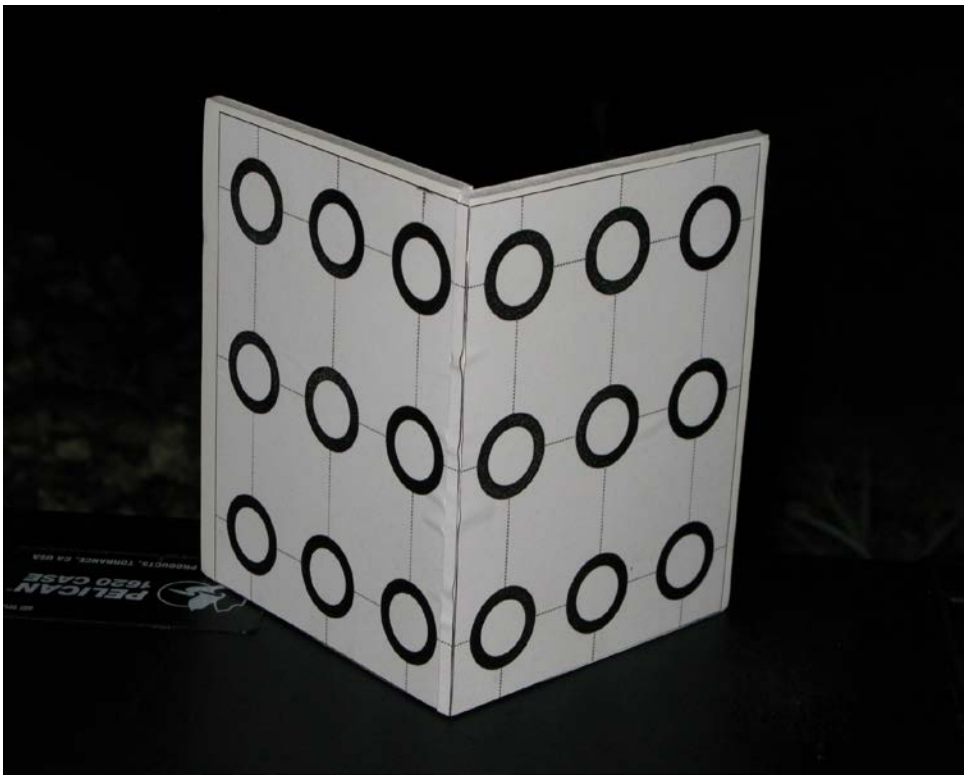

Figure 2.4The calibration grid.

Chapter 3
The Rotate And Hold And Scan SLI Technique

In this section, we introduce an SLI 3-D image acquisition technique called Rotate And Hold And Scan (RAHAS). An evolutionary introduction will be made with comparisons to previous techniques with brief explanations as to how RAHAS addresses common issues related to SLI. A conceptual overview will be necessary for comparison with previous techniques, with a list of RAHAS specific terms that set a common basis of understanding for thereader.The prototype scanning apparatus used for the scanner will be presented followed by the RAHAS processing algorithm in the last section in the chapter.

Section 3.1 Introduction

The RAHAS technique inherited its name from the Lock and Hold motion capture method [40, 41] since both involve a staged capture process and use stripe tracking as a method for tracking pattern variation. As the name implies, the Lock and Hold technique is broken up into two stages: Lock, and Hold. The first stage uses a PMP scan to get a "lock" on the 3-D surface depth information, and the second stage tracks the variation of a stripe pattern from target motion between successive frames to "hold" onto the 3-D surface changes. The stripes during the "hold" stages are identified using tracking algorithms, which are called "snaking" or "snake tracking."

Further similarities between RAHAS and previously developed techniques exist in the use of high frequency PMP patterns (f >10). While the multi-frequency PMP technique discussed in the previous section uses lower frequency scans to "unwrap" ambiguities, RAHAS uses stripe tracking borrowed from Lock and Hold as a method for removing

ambiguous phase information. This stripe tracking stage occurs during the rotation of the RAHAS pattern and is analogous to the "hold" process of Lock and Hold. This allows RAHAS the capability for the improved depth resolution of a Multi-Frequency PMP scan, but the simplicity of not requiring a computer controlled projector – RAHAS operates using a single pattern slide with mechanical rotation and translation stages.

Section 3.2 RAHAS Conceptual Overview

Rotate and Hold and Scan (RAHAS) is a SLI technique that uses snake [42] tracking to explicitly identify the projected pattern stripes so that the ambiguities from a PMP scan can be removed. The RAHAS process is named for the three stages that describe how the pattern is moved across the object-- Rotate, Hold, and Scan, but the initial Epipolar Alignment of the stripe pattern is what allows the identities of the stripes to be known. The term Epipolar Alignment refers to the orientation of pattern stripes along the line that is drawn through both the projector and camera optical centers. This alignment is important because it removes the depth variation of the stripes and they appear straight, which allows for explicit identification.

The Rotate and Hold and Scan (RAHAS) process begins with the analogous of "lock" which is the identification of the stripes while the pattern is in epipolar alignment. Analogously to the "hold" process, the sinusoidal pattern is then tracked through a rotation of 90 degrees from the epipolar direction to phase alignment, an orientation of maximal depth distortion. The phase alignment allows a translation of the sinusoidal pattern to yield a traditional Phase Measuring Profilometry (PMP) scan, and with the identities of the stripes, that correspond to the boundaries for the wrapped phase regions, the ambiguities of the PMP scan can be removed. The motion stages of the RAHAS capture process are summarized in Figure 3.1.

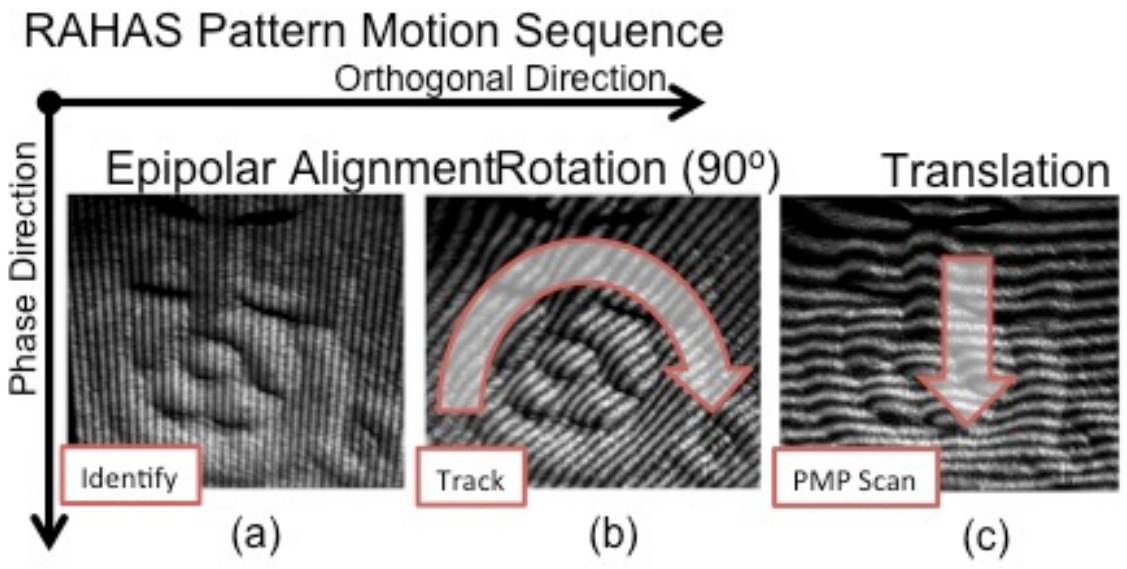

Figure 3.1 The pattern motion for a full capture sequence. a) The stripes in epipolar alignment. b) The rotation. c) The stripes are shown with maximal distortion, and occlusions can prevent the correct identification of stripes, if they were not already identified in part (a).

Section 3.3 RAHAS Hardware Description

The RAHAS prototype scanner has three main components: a video camera, a high-resolution camera, and a slide projector. The video camera captures the sequence of images during the pattern motion outlined in Figure 3.1, while the high-resolution camera is used to provide the image texture that will be mapped onto the generated 3-D surface using a technique called mixed-resolution (MxR) [44]. The high-resolution camera can optionally be removed for a more compact scanner apparatus, with the texture image being supplied by the video camera. The slide projector consists of a high lumen LED mounted in a tube with optical lens focusing the light through a mounted slide. The motion of the pattern is controlled through the use of a mechanical assembly with two controls: a lever for rotation and a crank for phase translation. The rotation is controlled manually by the physical rotation of a lever attached to the slide carriage mount, which allows for the full 90 degrees of rotation from epipolar alignment to phase alignment. A crank with an attached cam is used for the phase translational motion of the pattern. The

crank is turned which spins the cam and forces the slide projector's elevation angle to change based upon the eccentricity of the cam. Since the motion of the pattern is controlled manually, distortion is introduced to the resultant PMP scan based upon the velocity of motion of the mechanical system.

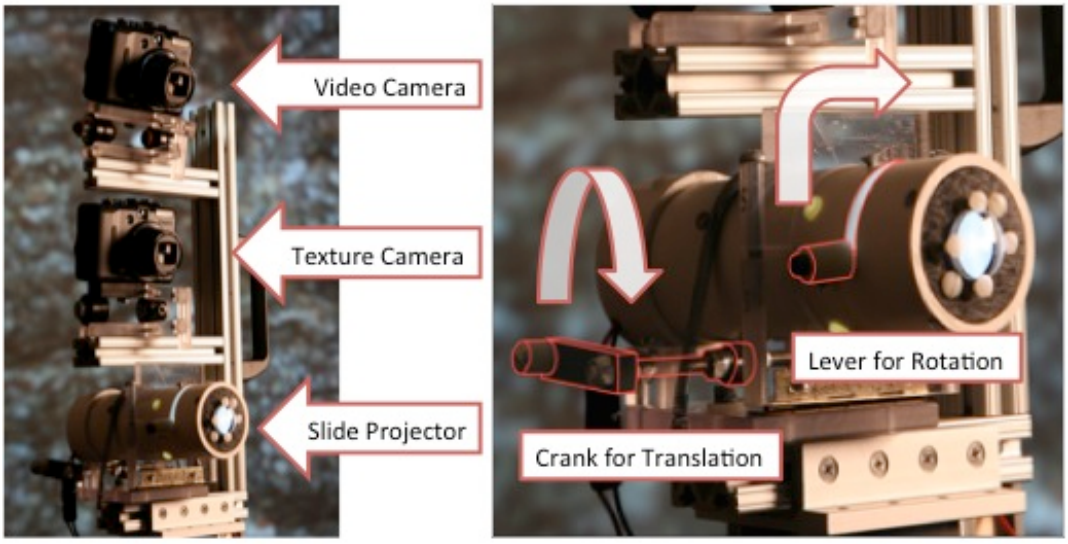

Figure 3.2 The RAHAS Prototype System. a) The complete system showing the three separate components: Video Camera, Texture Camera, and Slide Projector. b) The mechanical controls for the rotation and translation of the pattern.

3.3.1 Issues with the Prototype

The main beneficial characteristic of the RAHAS technique is that a digital camera and a simple slide projector are the only required components. While this allows the use of a scanner untethered to a computer, it also removes the synchronous control of projection and capture. From this lack of control arise differences with traditional PMP with a tethered computer. With traditional computerized PMP the projection and capture devices are controlled together, so when the projector is projecting a pattern of known incremental phase the camera can capture the specified phase shifts.

For example, the computer controlled PMP capture process can be thought of as a discrete-time systemof the projected patterns. The pattern that represents a specific phase shift is projected onto the object, the camera captures that image, and then the new pattern with incremented phase is projected. This is repeated until the pattern has been shifted a full period, and only those signals at distinct phase shifts are ever projected upon the object. In contrast, the RAHAS technique can be thought of as an analog-to-digital conversion. The process uses a slide projector, which is controlled with a hand-turned lever and crank, that continuously varies the phase of the pattern across the surface of the object. The camera captures the images of the pattern on the surface at discrete-time intervals related to the video rate of the camera. This is analogous to the discrete sampling of a continuous signal, but proves to be problematic since the captured images will likely not be sampling points that are evenly spaced in phase. The correction process used for this is discussed in Section 3.5.1.

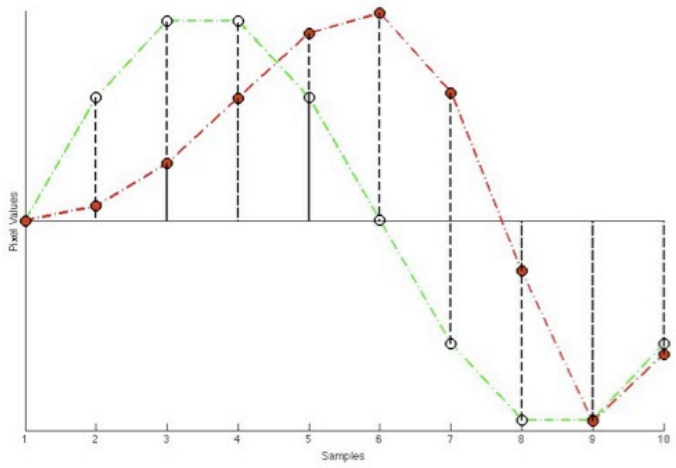

Figure 3.3 Time-varying signal at a pixel. A representation of the sinusoidal signal at a pixel, and how it changes with non-constant pattern motion. The signal in green with empty circles at the sample points is the ideal sinusoidal response, and what would be achieved with computer controlled PMP. The signal in red with filled in circles is the actual response of a pixel in the River Scan 2, that demonstrates the distortion from manual motion.

As opposed to the computer-generated PMP's succession of precisely shifted images, the RAHAS technique uses a manually controlled crank to control the phase-shift of the pattern. This manual control causes the translational motion of the projected pattern to

have non-constant motion, which causes the sinusoidally varying temporal responseof a single pixel to distort. The temporal response of each pixel is vital to the success of PMP because this distortion is frequency or time dependent, which can obscure the phase information for accurate identification of pixels in triangulation. The distortion can be characterized by a temporal compression or rarefaction of the expected sinusoidal shape, which is a change in the frequency spectra of the signal. Further discussion of this topic is presented in Appendix A.

Section 3.4 RAHAS Processing Algorithm:

This section discusses the RAHAS processing algorithm, and will be divided into sections that can be visualized in Figure 3.4. The first section is a pre-processing step that prepares the image data for snake tracking. Next is snake tracking, which is followed by the phase processing of the PMP scan.

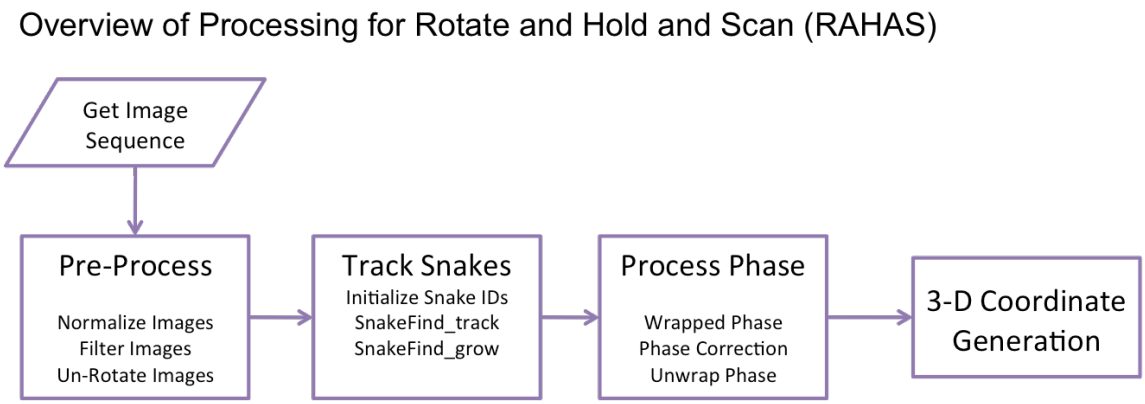

Figure 3.4 Overview flowchart of the Processing for RAHAS.

3.4.1 Pre-Processing the Images

The algorithm begins by loading and preparing a sequence of images that have captured the RAHAS pattern motion, described in the previous section. The sequence of images are normalized, to balance the slight variations when using an automatic camera, and

filtered, in order to remove noise and smooth the images for ease of snake tracking. Two filters are used, a median filter and a moving average filter, both with rectangular kernels.

After the images are filtered, a rotation is performed on each image in the sequence to orient their stripes to the phase direction, shown in Figure 3.5. The purpose of this "un-rotation" of the image sequence is to allow the peak detection to only have to operate in a single dimension. As the sequence progresses, the stripes distort, but retain the alignment. With low angular velocity of the pattern, the precise angle of “un-rotation” is not necessary because the stripes will distort with small changes between frames, and will be able to be tracked frame-by-frame.

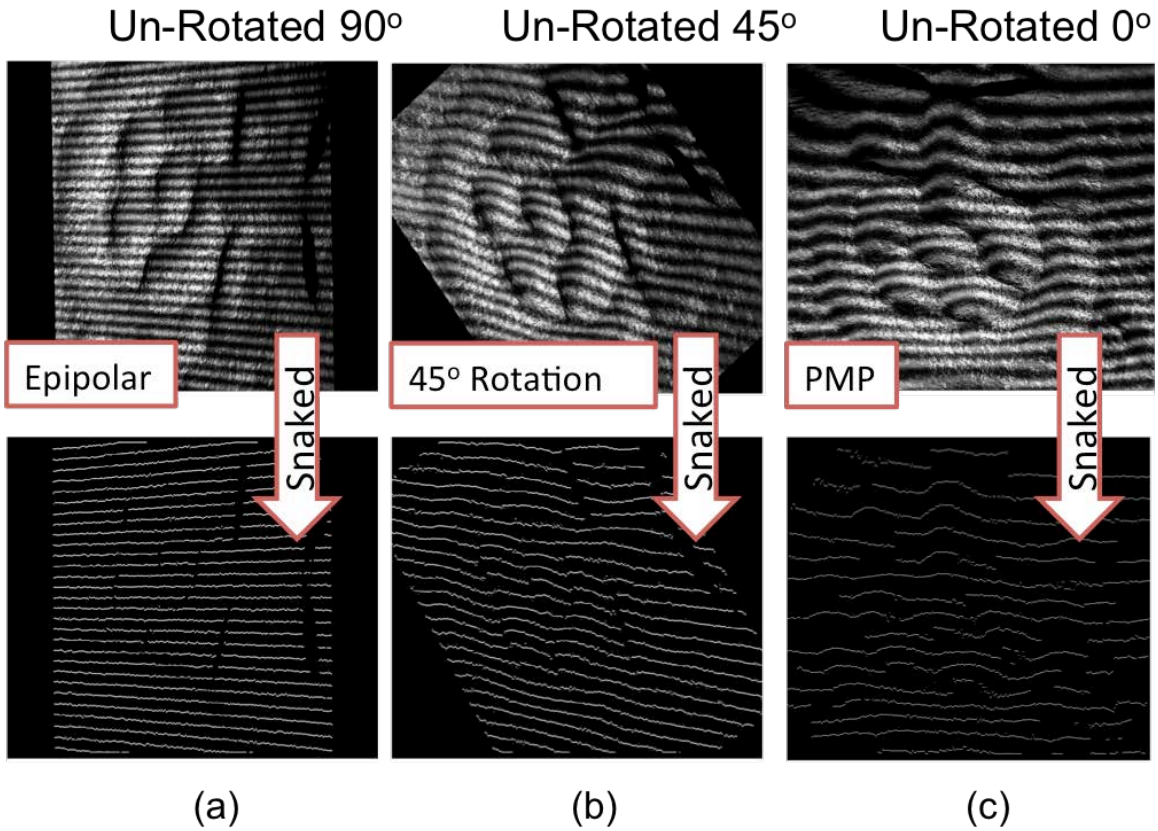

Figure 3.5 Unrotation pattern sequence. Demonstration of the “un-rotation” of the pattern sequence with the same images from Figure 3.1 (a, b, and c). The top is the image rotated so that the stripes are horizontal, and the bottom images are the snakes of the same image. At Epipolar alignment in the first frame of the sequence (a), the “un-rotation” angle is 90^{o}, while decreasing to an “un-rotation” angle of 0^{o} during the PMP scan (b).

The angle of rotation for each image in the sequence is determined by the equation

$$\theta_{rotation} = 90^o \frac{N-(n-1)}{N} \tag{3.1}$$

where*N* denotes the number of frames in the rotation sequence, and *n* is the frame index. The angles with relatively flat target surfaces could alternatively be determined using a 2-D FFT and measuring the angular displacement of the peaks corresponding to the sinusoidal pattern. This method worked well for image frames in which the stripes were straight, but when surface changes distorted the stripes to oblique angles, like what occurs when projecting onto the calibration grids, this approach does not work reliably.

Peak Detection and Snake Masking

The definition of a snake specifies that they be placed along the stripes of the sinusoidal pattern that is used for the PMP scan. In order to "snake" an image, the peak position of the stripes must be determined. The determination of the peak locations is by the usage of a peak-to-sidelobe-ratio (PSR) [41,43] operation performed on the image frame $A_i(x,y)$, and found in the function*anglePSR*. This function generates a separate image $A_{psr}(x,y)$ through the equation

$$A_{psr}(x,y) = \frac{A_i(x,y)}{Max\{A_i(x,y-r),\ A_i(x,y+r)\}} \tag{3.2}$$

where$r$is the expected sidelobe offset.

Next a function called *snakeMaskPeakPSR* generates the Snake Mask image, *D*, that has the position of the snakes in each image highlighted. The first step in the function *snakeMaskPeakPSR* is a thresholding operation on the PSR image, $A_{psr}(x,y)$, with user defined minimum PSR value, min_A, and minimum pixel value of *A*, min_{psr}, such that

$$A'_{psr}(x,y) = \begin{cases} A_{psr}(x,y) & where\ A_i(x,y) \geq min_A\ and\ A_{psr}(x,y) \geq min_{psr} \\ 0 & otherwise \end{cases} \tag{3.3}$$

Next, a vertical search is performed on the resulting thresholded image, A'_{psr}, to find regions of non-zero values, so that the maximum values in these regions can be determined such that the region *S* is defined by

$$\begin{gathered} S \in \{s_0, s_0+1, \dots, s_1-1, s_1\} \ where \ \ s_1 > s_0 \\ and \\ A'_{psr}(x, s_0-1) = 0 \ and \ A'_{psr}(x, s_1+1) = 0 \ \ and \ \ A'_{psr}(x, S) > 0 \end{gathered} \tag{3.4}$$

withs_0 as thelower bound and s_1 as the upper bound of the region *S*.

The binary encoding is defined by

$$\begin{gathered} D(x,y) = 255 \\ where \\ A'_{psr}(x,y) = Max\left\{v \middle| v = A'_{psr}(x, y+S) \ and \ S \in \{s_0, s_0+1, \dots, \ s_1-1, \ s_1\}\right\} \end{gathered} \tag{3.5}$$

so that the resultant image is the binary Snake Mask image, *D*, that has zeros everywhere, except where the PSR of the image frame A has local maxima. These local maxima correspond to the centers of the stripes in the sinusoidal pattern, and the location of snake pixels that will be named and tracked.

3.4.2 Snake Matrix Initialization

Snakes are initially identified in the first frame of the sequence with the function *SnakeFind_init2Snake*, which operates on the image *D* after the number of snakes and their spacing is determined. The *findNumSnakes* function generates the number and the spacing of the snakes by using a 2-D FFT on the first frame, the frame with undistorted stripes, to determine the frequency of the sine pattern.

The Snake Mask *D* is processed using *SnakeFind_init2Snake* to label the snakes in a narrow vertical band in the middle of the image. The function *collapseSlice* is used to average the location of the snakes in the *D* matrix to give a position for the start of the search algorithm.

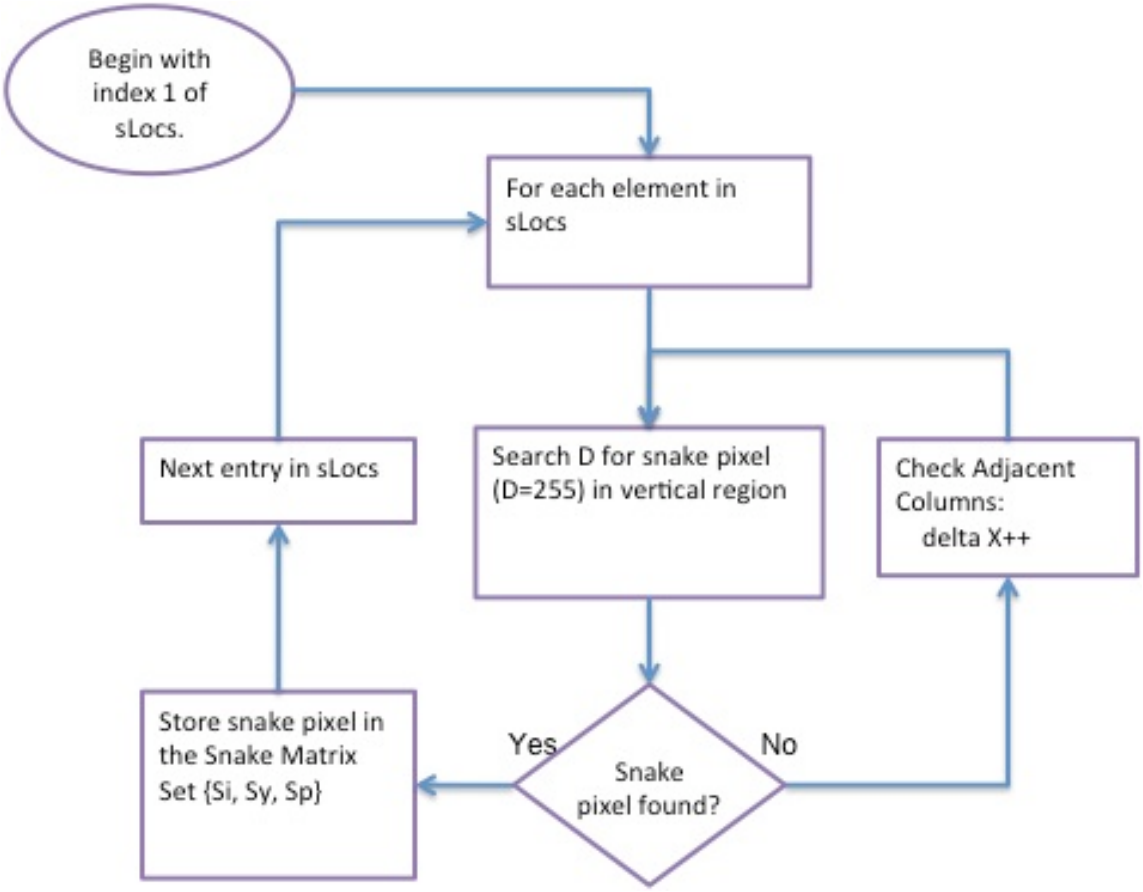

Figure 3.6 Flowchart of the SnakeFind_init2Snake function.

With the width of the image, N_x, the midpoint is $x_{mid} = floor\left(\frac{N_x}{2}\right)$. The collapse equation can be described by the equation

$$r_s(y) = \sum_{i=-d_m}^{d_m} D(x_{mid} + i,\ \ y) \tag{3.6}$$

where$d_m$is the radius, in the x-direction, of the vertical band about the midpoint. The output r_s is a 1-D vector that is searched by the function *findCollapsePeaks*to find where the summations from the collapse were the largest. The search process can be described by

$$r_{peaks}(y) = \begin{cases} 1 & \begin{matrix} where \quad r_s(y) > r_s(y \pm 1) \\ where\ r_s(y) = r_s(y+1)\ and\ \ r_s(y) > r_s(y+2)\ and\ \ r_s(y) > r_s(y-1) \\ where\ r_s(y) = r_s(y+1)\ and\ r_s(y) = (y+2)\ and\ r_s(y) > r_s(y-1)\ and\ \ r_s(y) > r_s(y+3) \end{matrix} \\ 0 & otherwise \end{cases} \tag{3.7}$$

where$r_{peaks}$is a 1-D vector that has length *My*, the height of the image, and has a value of 1 where the snakes are located. Since the indexes into $r_{peaks}(y)$ correspond to *y*-coordinates in the center column of the image, the final step is to store all the indexes (or y-coordinates of the snakes) that have been flagged as a snake into the vector s_{locs}. This allows the recovery of the snake y-coordinate values by iterating through the elements of the vector s_{locs}, and serves as a starting point for the region searched in the next part of this algorithm. This region is defined by a fixed maximum distance in the vertical direction, $deltaY = 10$ pixels, and the horizontal direction, $deltaX = 5$pixels, although the pixels are searched starting with the central points column and only searching adjacent columns if no snake pixel is found. An overview of the process can be seen in Figure 3.5 and the mathematics can be characterized by

$$\begin{aligned} Si_n(x_{mid} + j_o, i) &= i \\ Sy_n(x_{mid} + j_o, i) &= s_{locs}(i) + k_o \\ Sp_n(x_{mid} + j_o, i) &= A_n(x_{mid} + j_o, s_{locs}(i) + k_o) \end{aligned} \tag{3.8}$$

$$else\ 0$$

$$where\ [j_o, k_o] = Min\left\{ j,k \middle| \begin{matrix} D_n(x_{mid} + j, s_{locs}(i) + k) = 255 \\ and -5 < j < 5\ and -10 < k < 10 \end{matrix} \right\}$$

The result of the *SnakeFind_init2Snake* function is the labeled identity of each snake, although only for a single pixel. The next step is to "grow" the snakes from these single pixels.

3.4.3 SnakeFind_grow[Left|Right]

Now that there is a single pixel identified for each snake, these lone pixels can be "grown" horizontally to fill out the rest of the snake in *Si*. The snakes will be expanded by a single pixel at a time, until the end of the image has been reached, an annomally prevents snake detection, or a large shadow exists on the object to prevent growth. This expansion process is performed by the functions *SnakeFind_growLeft*and*SnakeFind_growRight*, which will also be used to fill in holes in the snakes during the snake tracking. While we will discuss the algorithm specifically for *growRight*, the only difference between the two (*Right* or *Left*) is a change of orientation.

The equations describing the *growRight* process are as follows

$$Si_n(x, m_s) = \begin{cases} 1 & if \quad Si_n(x-1, m_s) > 0 \quad and \quad D_n(x + j_o, y + k_o) = 255 \\ 0 & otherwise \end{cases}$$

$$where\ [j_o, k_o] = Min\left\{ j, k \;\middle|\; \begin{array}{c} D_n(x_{mid} + j, s_{locs}(i) + k) = 255 \\ and\ 0 < j < x_{mgrow} \quad and \quad -y_{mgrow} < k < y_{mgrow} \\ and\ y = Sy_n(x, m_s) \end{array} \right\} \tag{3.9}$$

wherex_{mgrow} and y_{mgrow} are values that define the maximum distances to search in their respective directions.

The *grow* functions begin by searching through a snake row in the *Si*matrix looking for the "end" of a snake, which corresponds to the current pixel being "blank" ($Si(x, m_{snake}) = 0$) and the previous pixel being "active" ($Si(x, m_{snake}) > 0$). When the "end" of the snake is found, a search is performed for the "valid" ($D(x, y) = 255$) snake pixel in the Snake Mask *D* with minimum distance to the location of the active pixel at the end of the labeled snake. This search of *D* starts at the current pixel's column, x, and the previous "active" pixel's *y* coordinate, determined from the *Sy* matrix $y = Sy(x \pm 1, m_{snake})$. The search progresses in single pixel increments, both up and down, until a valid pixel is found, or a *y*-search limit has been reached. If the *y*-search

limit has been reached, then the search continues in the next column (in the direction of the grow) starting at the same *y* coordinate and repeating the vertical search. This is repeated until a valid pixel is found in *D* and stored into $\{Sp, Sy, Si\}$, or the *x*-search limit is reached, in which case the current "end" of the snake is left alone and a new "end" is sought to repeat the same process. Using the *SnakeFind_grow[Left|Right]* functions, whole snakes can be formed in the initial image, and the tracking of the snakes can begin.

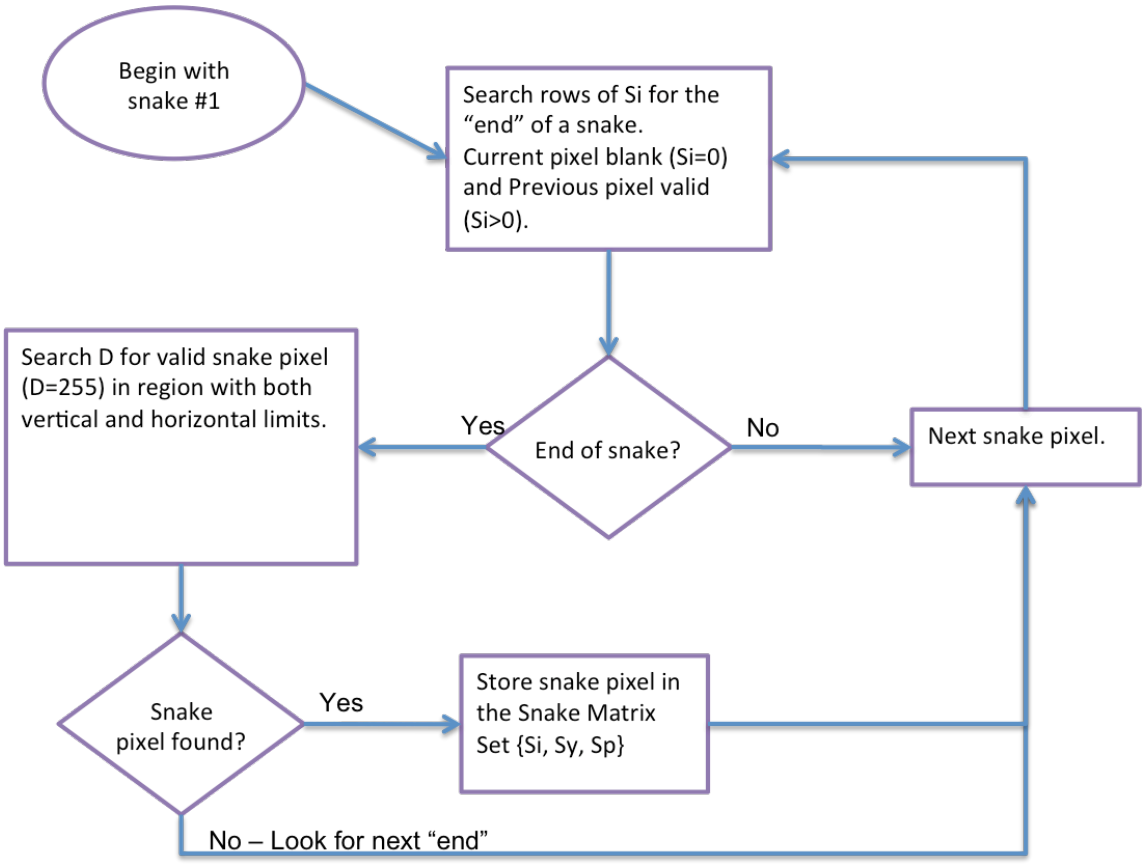

Figure 3.7 Flowchart of the *SnakeFind_growLeft/Right* function. The horizontal direction of grow corresponds to the name of the function: left or right.

3.4.4 Snake Tracking

Due to the orientation of the snakes in the horizontal direction (from the "un-rotation" of the images) and the slow movement of the pattern relative to the image capture rate, a snake pixel is assumed to only shift a small amount in its column between image frames. These small variations allow a search in the snake pixel's column to find the

location that the snake pixel has shifted, as long as the shift was within a maximum allowable distance. By finding the position of each pixel in the snake after it has shifted, the snakes can be tracked between two frames. If this is continued frame after frame, snake tracking in a whole sequence of images can be accomplished. An overview of the whole snake tracking process is presented in Figure 3.8.

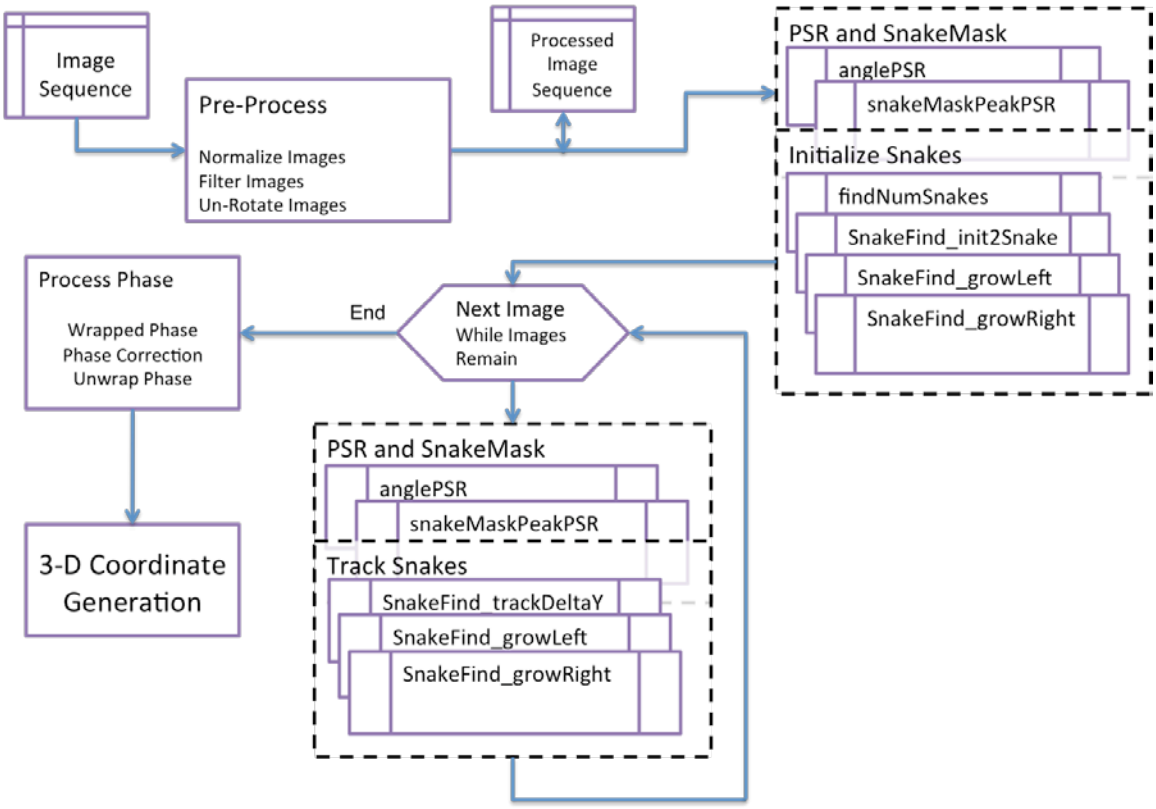

Figure 3.8 Flowchart overview of the snake tracking process for RAHAS.

The *SnakeFind_multiPassTrackDeltaY* function performs snake tracking after the first frame's snakes have been identified, and continues through the whole image sequence. The notation used for the sequence is as follows: *n*, denotes the current frame, and *N*, denotes the total number of frames. The snakes are tracked by comparing the marked pixels in the Snake Mask of the current frame (D_n) to the snake pixels in the Snake Matrices of the previous frame $\{SpB4, SyB4, SiB4\}$, and determining whether the snake pixel identified in the previous frame has moved within a maximum acceptable

vertical distance (y_{mtrack}) in its respective column. The equations describing this function are as follows

$$Si_n(x, m_s) = \begin{cases} 1 & if \quad Si_{n-1}(x, m_s) > 0 \quad and \quad D_n(x, y + k_o) = 255 \\ 0 & otherwise \end{cases}$$

$$where\ k_o = Min\{\, k \mid D_n(x, y + k) = 255 \quad and \quad -y_{mtrack} < k < y_{mtrack}\} \quad (3.10)$$
$$and\ y = Sy_{n-1}(x, m_s)$$

wherem_s is the snake that is currently being operated on, which also corresponds to the row of the Snake Matrices, and y_{mtrack} is the maximum distance to search in the vertical direction.

The multiPass designation means that the process was performed twice, once starting with the first snake and proceeding top-down, and a second time starting with the last snake, and proceeding bottom-up. Both of these snake matrices are generated, compared, and only the pixels that tracked the same in both passes are kept, or the output is the intersection of the sets of "top-down" and "bottom-up". The *multiPass* process can be characterized by

$$Si_n = Si_{nDown} \cap Si_{nUp} \quad (3.11)$$

whereSi_{nDown} and Si_{nUp} are both determined from Equation 3.10, but using opposite directions for processing the snakes. Si_{nDown}begins at the top and works down (from snake 1 to *N*), while Si_{nUp} begins at the bottom and works up (from snake *N* to 1).

The algorithm begins at either the first snake or the last snake in the previous frame's snake matrices {*SiB4, SyB4, SpB4*} depending on the pass direction that is being processed, with the other direction to be processed after, and the intersection of both passes as the final result. For each snake (m_s) in the snake matrix SiB4, the snake pixels are looped through and processed if the pixel is active *(SiB4(x, m_s) > 0)*. When an active snake pixel is found, the snake pixel's image *y*-coordinate, *y = SyB4(x,m_s)*, is used as a

starting point for a search in the current Snake Mask $D_n(x,y)$. The search progresses in single pixel increments, both up and down, until a valid pixel is found, or the *y*-search limit (y_{mtrack}) has been reached. If a valid pixel is found then it is stored in the current Snake Matrix set $\{Si_n, Sy_n, Sp_n\}$, and the process proceeds to the next snake pixel. The process also proceeds to the next snake pixel if the search reaches the limit without finding a valid pixel in the Snake Mask. This continues through all the pixels in the current snake, then checks the subsequent snakes (either above or below depending on the pass direction). After all the snakes in a frame are processed, and the intersection of the *multiPass* has been determined as in Equation 3.11 the function *SnakeFind_multiPassTrackDeltaY* generates a set of Snake Matrices that correspond to the current frame $\{Si_n, Sy_n, Sp_n\}$. This set of Snake Matrices is processed with *SnakeFind_multiPassGrow[Left|Right]*, as discussed above, but with a *multiPass* addition, to attempt at filling in any holes that could not be tracked. Now the Snake Matrix set $\{Si_n, Sy_n, Sp_n\}$ is stored as the previous set {*SiB4, SyB4, SpB4*}, and the current frame is incremented -- the process repeats to the end of the image sequence.

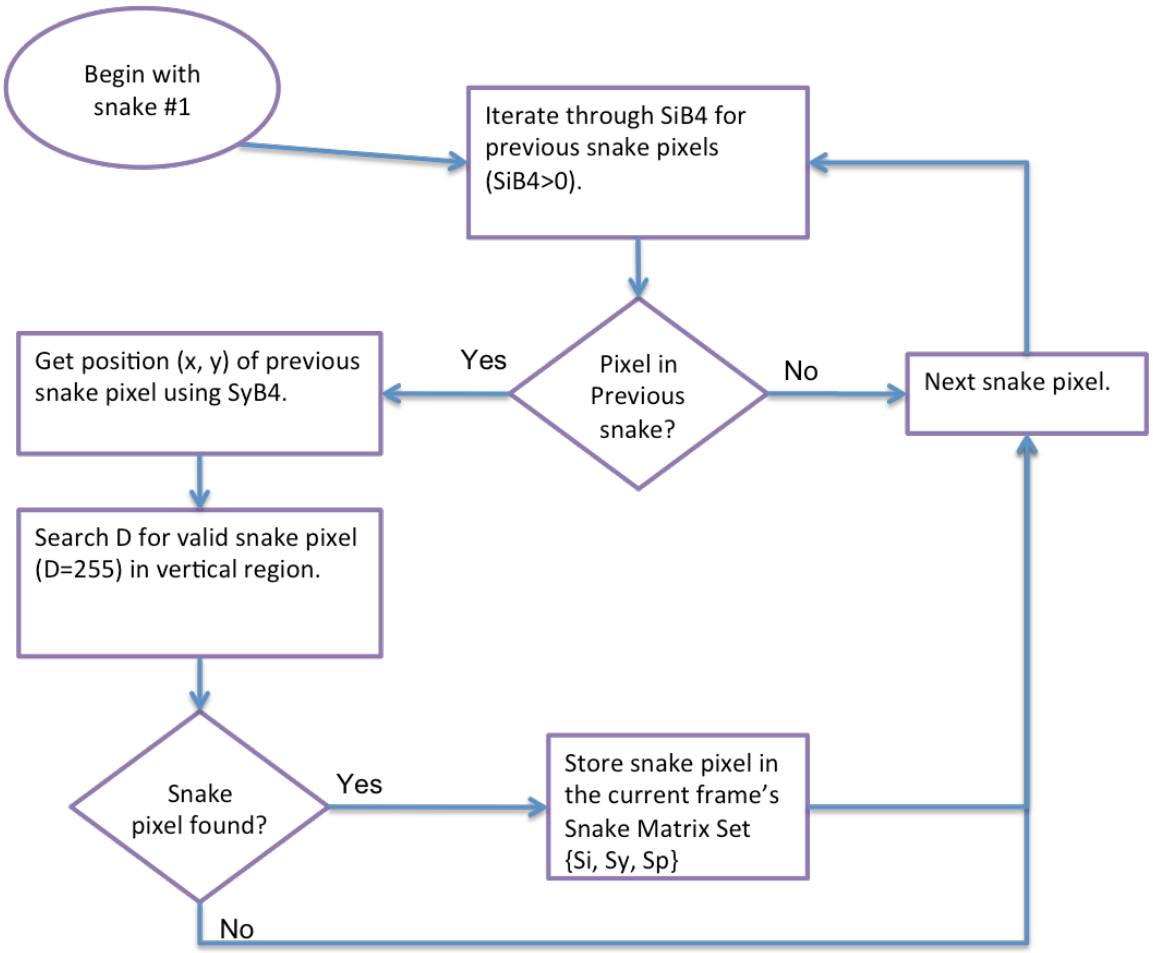

Figure 3.9 Flowchart describing the *SnakeFind_trackDeltaY* function.

Section 3.5 PMP Scan and Phase Processing

The phase processing begins after the snakes have been tracked through both the rotation and translation of the sinusoidal pattern, and the snake positions in the image plane are known explicitly. The snake positions will be used in the unwrapping stage to remove the ambiguities of the high frequency PMP scan, and in the estimation of pattern motion used in the correction process. The motion of the sinusoidal pattern (translation in the phase direction) defines the PMP scan stage, but a problem arises due to the motion generated by a hand turned crank. The velocity of the pattern is not constant, so the frame captures of the video camera are not uniformly spaced in the phase of the sinusoidal pattern. As discussed in Chapter 2, the PMP equations call for equally

distributed phase values, so a process is performed to "correct" the phase for use with traditional equations.

3.5.1 Phase Algorithm

The Phase processing begins with determination of the frames in the PMP sequence. The first frame of the PMP sequence is chosen manually by visual inspection of the video sequence for the frame in which the translation is first noticeable, but the actual number of frames must be determined using the snake positions of this first frame. Using the definition of the pattern as a sinusoid and the location of the snakes at the peaks of the sinusoidal pattern, the vertical distance between two adjacent snakes should be the phase equivalent of 2π, or a single period of a sine wave. Taking advantage of this relationship allows the snake locations to determine when the pattern has moved a distance that would correspond to a full period, and will give the final frame of the sequence.

In the first frame, the *y*-coordinate of a snake is defined by $y_0 = Sy_0(x, m_{snake})$, and the *y*-value that would correspond to a translation of 2π is the next snake's *y*-coordinate $y_N = Sy_0(x, m_{snake} + 1)$. The *x* denotes the column, and must be the same. After the initial and final *y*-values are determined from the first frame (denoted by the 0 subscript), the *y*-value of the same snake in subsequent frames will be compared to y_N, the *y*-value corresponding to a phase of 2π. The current frame's *y*-value is described by

$$y_n = Sy_n(x, m_{snake}) \tag{3.12}$$

where$n$ corresponds to the current frame index. The frame index starts at 1, the first frame after 0 phase, and continues until the boundary of 2π is reached as explained by

$$n \in \{1,2,\dots,k\} \; where \; Sy_k(x, m_s) < y_N < Sy_{k+1}(x, m_s)) \tag{3.13}$$

k is the last frame of the PMP sequence just before the *y*-value passes y_N. The Equations 3.12 and 3.13 define the search criteria for finding the end of the PMP sequence, as well as simultaneously performing a task to construct the per frame phase shift estimate, ϕ_n.

$$\phi_n = 2\pi \frac{y_n - y_0}{y_N - y_0} \tag{3.14}$$

The phaseshift estimate between frames is based upon the snake distance moved per frame as a percentage of the total distance between snake m_{snake} and the adjacent snake $m_{snake} + 1$ corresponding to the percentage of total phase. $\phi_n$is the actual phase shift per frame and will be used to interpolate the images $I_n(x, y)$. A visual representation of this phase shift estimating process is shown in Figure 3.9. The sinusoidal pattern represents the projected pattern with tracked snakes superimposed on top. The triple lines are the snakes in the initial frame 0, and the dashed lines represent the position of snake m_{snake} in each of the subsequent frames denoted by the subscripts(*0, 1, 2, … ,n*).

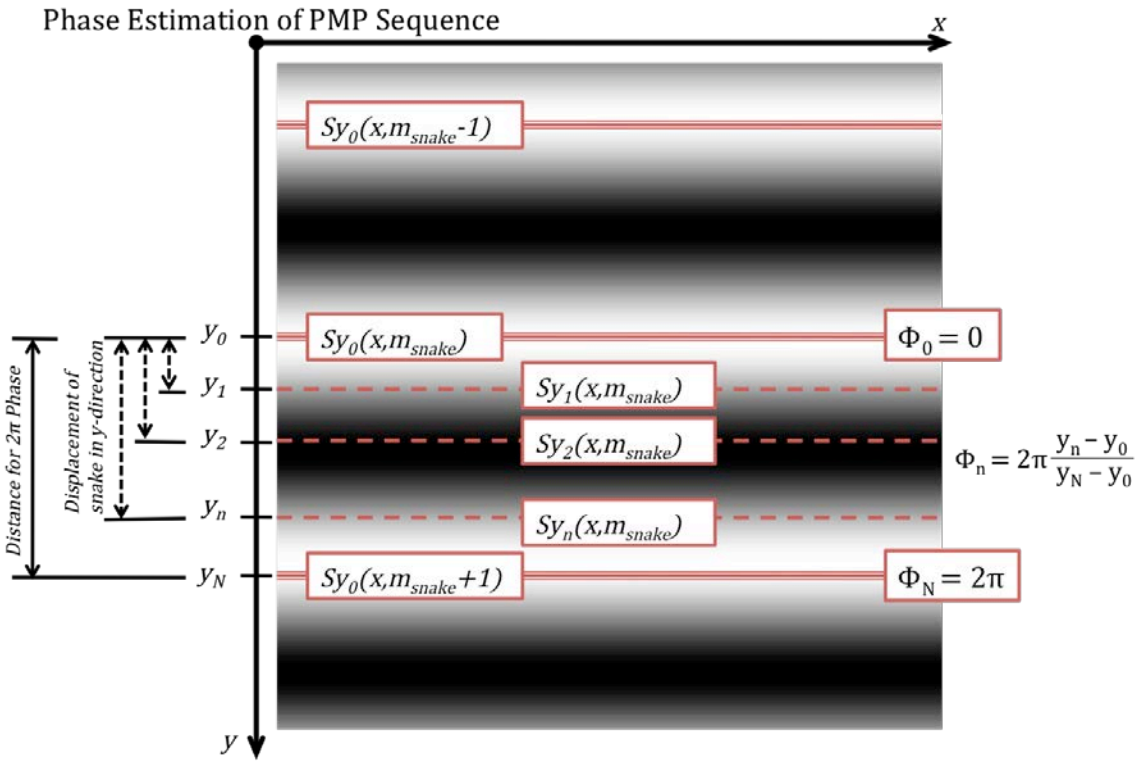

Figure 3.10Phase Estimate Example. Visual Representation of how the phase is estimated for each frame in the PMP sequence. The left side shows the change in the y-values of the snakes in the image pixels, while the right side shows the phase assigned for each snake.

Phase Correction by Interpolation

In order to use the well-known PMP equations discussed in Chapter 2, the image values, $I_n(x, y)$, need to be corrected and interpolated to the values at the uniformly distributed phase values described by

$$\theta_n = \frac{2\pi n}{N} \tag{3.15}$$

whereθ_n is the desired or corrected phase values per frame, n is the frame index and N is the total number of frames in the sequence. The interpolation process alters the pixel values in each image of the sequence using the following equations:

$$\alpha = \frac{\phi_{m+1} - \theta_n}{\phi_{m+1} - \phi_m} \quad where \;\; \phi_m < \theta_n < \phi_{m+1} \tag{3.16}$$

and

$$I_{int,n}(x, y) = \alpha I_m(x, y) + (1 - \alpha) I_{m+1}(x, y) \tag{3.17}$$

where$m$ is an index for the actual phase values denoting the indexes above and below the index n of the desired phase index. With the corrected images that are uniformly spaced in phase, the traditional PMP equations can be used.

3.5.2 Generate Wrapped Phase

As presented in Chapter 2, the equation for the wrapped phase is

$$\phi_w(x^c, y^c) = arctan\left[\frac{\sum_{n=0}^{\mathrm{N}} I_{int,n}(x^c, y^c)\sin(\theta_n)}{\sum_{n=0}^{\mathrm{N}} I_{int,n}(x^c, y^c)\cos(\theta_n)}\right] \tag{3.18}$$

and the equation used for the quality image can be described as

$$Q(x,y) = \sqrt{\left(\sum_{n=0}^{\mathrm{N}} I_{int,n}(x^c,y^c)\sin(\theta_n)\right)^2 + \left(\sum_{n=0}^{\mathrm{N}} I_{int,n}(x^c,y^c)\cos(\theta_n)\right)^2} \quad (3.19)$$

The Q image acts as a measure for how good the scan is based upon the peak-to-peak temporal variation of the patterns at each pixel. The Q image should be a gay level image without the appearance of stripes or bands, and for traditional PMP this is the case, but for RAHAS bands are present and have not been able to be removed completely. This banding phenomenon will be discussed later.

3.5.3 Unwrap the Phase

Now that the wrapped phase has been generated it must be unwrapped in order to combine the repeated phase bands into a whole phase image. As discussed earlier, the snakes are used to determine the boundaries of the wrapped phase image, but the first step is to linearly generate the correct phase at each snake boundary by the equation

$$\theta_k = 2\pi\frac{k-1}{M_s} \quad (3.20)$$

Equation 3.20 assumes a phase of zero at snake $k = 1$, and a phase of 2πat the last snake M_s, which is the total number of snakes that were in the slide pattern. The phase is going to be used to map positions in the camera space to the projector space for triangulation, and we assume 0 phase at the top of the slide pattern, and 2π at the bottom of the slide pattern.

With the phase of each snake known in the projector space, the snakes are used as boundaries to unwrap the bands of the wrapped phase image. The unwrapping of each band is performed pixel-by-pixel and band-by-band by the equation

$$\phi_{UW}(x,y) = \begin{cases} \theta_k + \dfrac{\phi_w(x,y)}{M_s} & where \quad Sy_0(x,k) \le y < Sy_0(x,k+1) \\ 0, & where \quad |Sy_0(x,k) - y| < 4 \end{cases} \quad (3.21)$$

inwhich$k$ represents the current boundary, θ_k is the phase at the boundary, as determined from Equation 3.20, and the pixels within 4 pixels of the boundary are zeroed out to prevent discontinuous phase at the boundaries. For each band, the wrapped phase, ϕ_W, is simply added to the constant phase. Figure 3.10 shows a typical wrapped phase image and the corresponding unwrapped phase image generated using Equation 3.21.

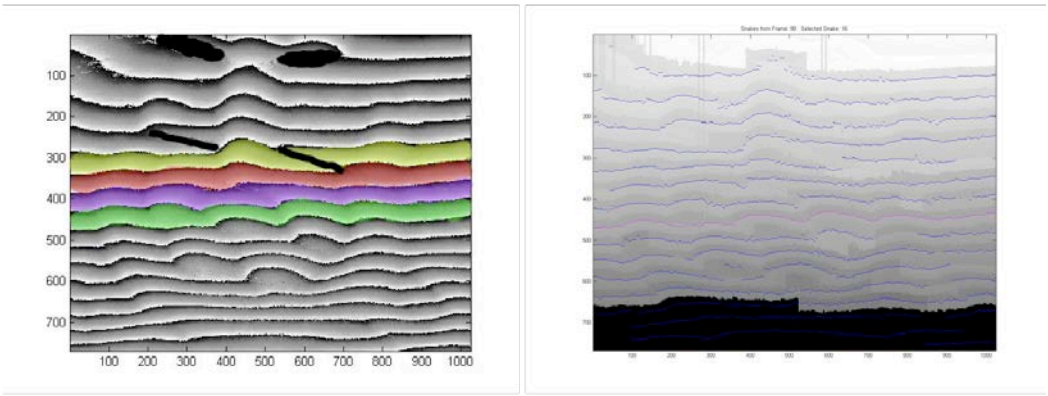

Figure 3.11 The phase images: (a) wrapped phase and (b) unwrapped phase. The wrapped phase image (a) is shown with four of the phase bands colored.

A single column of the phase images is presentedas further explanation of the unwrapping process. The cross-sectional view shown in Figure 3.11a shows the "repeated ramp" shape that is characteristic of wrapping phase, with each ramp corresponding to a specific phase band. In Figure 3.11b, the wrapped phase is shown on the same axis as the unwrapped phase ramp. Notice that the shape of both signals is identical in each vertical band corresponding to the wrapped bands of phase, and "repeated ramp" wrapped phase would be completely identical if each ramp had the corresponding phase value offset as detailed in Equation 3.21.

Since the unwrapped phase ϕ_{uw} is linearly distributed in the phase direction of the projector coordinates, the Equation 2.4 shows the relationship between the $\phi_{uw}(x^c, y^c)$ phase image and a corresponding column on the projector image planey^p. The x-coordinate of a specific pixel (x^p, y^p) along the column of the projector image plane equals the x^c coordinate due to the symmetry oftheepipolar alignment of the projector

and camera. Using Equation 2.17 the vector (x^c, y^c, y^p) generates a corresponding 3-D world coordinate point (X^w, Y^w, Z^w).

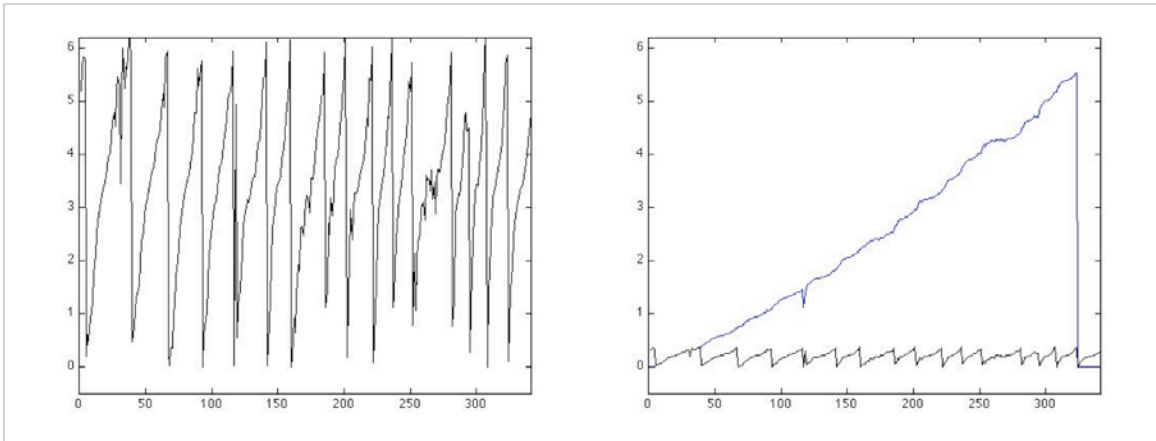

Figure 3.12 Phase Cross-Sections. (a) The cross-section of the wrapped phase at the center column. (b) The unwrapped phase cross section (blue) is shown along side the wrapped phase cross section (black) to demonstrate how the unwrapped phase is a copy of the wrapped phase signal detail in each phase band.

Chapter 4
Expeditionary and Experimental Results

As mentioned in Chapter 1, RAHAS is by design a SLI technique that can be used in remote locations; therefore, to test the usefulness of a RAHAS system in the field and gather some real data, a prototype system was developed and brought on a whitewater-rafting trip down the Rio Platano, Honduras to visit a few of the archaeological sites along the river. The purpose of this chapter is to present the results of applying the RAHAS processing algorithm (detailed in Chapter 3) on the actual data for which it was developed.

The first sectiondescribes the jungles of Honduras and how the sites were decided upon. The next section gives an overview of the journey to the specific archaeological sites, and briefly describes the individual sites and what was scanned. The third section discusses issues related to capture of 3-D scans in a tropical jungle and how these challenges were addressed. Next the procedure for scanning with the RAHAS Prototype system is presented, and the review process of the data is explained. The results of the RAHAS processing applied to real data are unveiled in the last section.

Section 4.1 Location of Archaeology Field Work

The field scanning took place during the summer of 2009 in the Rio Platano Biosphere Reserve, which is protected as one of 180 natural World Heritage Sites by UNESCO (United Nations Educational, Scientific and Cultural Organization). The reserve accounts for the largest tract of virgin tropical rain forest in the northern hemisphere, and boasts immense biodiversity with countless species of both flora and fauna. The region also encompasses a diverse array of ecosystems with humid semi-mountainous tropical forests

inland, lush coastal plains and mangrove forests along the Caribbean shoreline, with savannas in-between.

Figure 4.1 Map of Honduras. Shows the location of the Rio Platano Biosphere and the major cities.

The Rio Platano Biosphere Reserve is part of a larger geographical region called La Mosquitia, or The Mosquito Coast, which runs along the Caribbean coast of Honduras and Nicaragua. Despite sharing the name with a certain bothersome insect, The Mosquito Coast is actually named for one of the native peoples that live there called the Miskito. La Moskitia is also home to three other distinct indigenous groups – the Pech, Garifuna, and Tawahka – each with their own unique languages, cultures and traditions. These indigenous groups make up the primary residents of this remote sparsely populated region, as well as being the descendants of the purveyors of material culture at the sites visited during the expedition.

Instrumental to the success of the fieldwork was La Mosquitia Archaeologist Dr. Christopher Begley, whose 15+ years of conducting research and serving as a guide into

the Rio Platano Biosphere provided the knowledge and expertise to make the 3-D scanning foray into this remote jungle happen safely. Through Dr. Begley's experience, the sites to be visited were chosen based upon ease of access and the likelihood of finding material culture to scan. Since potshards and grinding stones in good condition were frequently plundered from these sites, finding complete artifacts was uncertain. Dr. Begley chose three archaeological sites, with the first two used predominately as practice in preparation of the third site. The three sites visited were a cave, a hillside settlement, and a river island with petroglyphs on rocks among shallow waters. The goal of the expedition was to visit the third site and capture scans of the petroglyphs, or pictorial carvings, that are on the rocks found along the Rio Platano.

Section 4.2 Expedition

The trip consisted of multiple legs, but started in the capital city of Honduras, Tegucigalpa. All-terrain vehicles were driven for a day towards the border region of the reserve and that night was spent in the village Bonanza. The following morning the gear was loaded on to mules and carried 10 miles to the headwaters of the Rio Platano. For packing on a mule train, it is important that the system could handle impact shock and abrasion because the mules are largely inconsiderate to what they carry and tend to bang, scrape and crash through obstacles in their path.

The next day the gear was loaded into small, inflatable whitewater rafts (Aire Pumas), the primary mode of transportation through the Biosphere, and the longest leg of the journey began. The Rio Platano at the headwaters was small only around 20-30 feet across with many rocks protruding the surface. The water was relatively low, so the raft would periodically become stuck on rocks in the shallow water. The low water made maneuvering rapids slightly more difficult and it was only a few hours into the trip that the raft with the system caught a rock while navigating a rapid and flipped over. This would not be the last time that the system was submerged in water, but due to the watertight Pelican case it would not matter.

4.2.1 Archaeology Sites – The Cave on Cave Creek

After a day of paddling on the Rio Platano, the campsite closest to the first archaeological site was reached shortly before dusk. The next morning the Pelican Case containing the RAHAS prototype was carried an hour and a half up a trail to the cave that contained the first archaeological site. The entrance to the cave followed the creek for which it was named, Cave Creek, back into the earth.

Inside the cave was a raised area that was out of the water. Strewn about the area were the remnants of pots and grinding stones, made of various types of stone. The bottom of a three-legged grinding stone was scanned twice, with each of a different perspective with the hopes of combining the 3-D surfaces into a complete object.

4.2.2 Archaeology Sites –The Hill Side Site, Los Metates

At midday of the following day, the second archaeological site was reached. The site was called “Los Metates” and was located on the side of a hill that overlooked the Rio Platano near the mouth of the Rio Camalotal. Recent rains had caused a mudslide that washed away part of the shore and fallen trees lay in the water making disembarkment difficult.

Once at the site, a black tarp and some cut bamboo lengths were used to construct a make-shift tent to block out the sunlight. A small three-legged grinding stone was placed on the pelican case inside the tent, and scanned twice with the hope of merging the scans together at some later date.

4.2.3 Archaeology Sites –The River Petroglyphs at Walpaulban Tara

After three days of paddling, the third and final scanning site was reached. This rocky area with shallow pools was surrounded by the Rio Platano and named Walpaulban Tara. What was to be scanned here was different from the two previous sites, and since the petroglyph carved rocks were only a few hundred feet from where camp was set up, more time could be allocated for both calibration and scan. This extra time spent on scanning resulted in the best scans.

Water pools were all through the rocky area varying in size from small puddles to a depth of 4 feet. Due to this water throughout the area, the site was surveyed prior to scanning so a plan of action could be made. The plan was to choose three petroglyphs to scan, and wait until dark to carefully carry the pelican case to the sites. Each petroglyph required the construction and deconstruction of the scanner back into the box in order to move it safely among the pools inside the waterproof case. Once out of the case and assembled, the scanner was carefully carried over water to the three separate sites, leaving the case on dry ground.

Section 4.3 RAHAS in the Jungle

Using the RAHAS prototype scanner in the jungle is challenged by both the physical harshness of the environment, and the introduction of ambient sunlight when working outside. As an alternative to designing a ruggedized prototype, the system was packed in a single Pelican case. The Pelican case was watertight and had ample shock absorbing foam with custom molded compartments for each piece of the disassembled prototype. This served as both protection and a carrying case with which the system was transported. Although the packed case weighed in at 50 lbs. the system proved manageable in packing to and from the archaeological sites that were dispersed along the length of the river. The prototype system survived the whole trip unscathed.

In order to use Structured Light Illumination, the projected pattern needs to be the main luminous source of a target object to get proper contrast for pattern differentiation. When used in labs, sufficient brightness is reached both by turning the room lighting off and having higher output projectors running off AC line power. In contrast, when used outdoors the ambient light cannot be removed as easily, and lower-powered projectors are used that run on batteries. The study of sufficient projector brightness in Structured Light is beyond the scope of this thesis, but make note that the typical AC powered projector produces 1000-3000 lumens, while the RAHAS prototype used a single battery

powered LED that produced 120 lumens. Lumens are a flux measurement for light intensity, and if divided over an area the lumens will yield the unit Lux (lumens/area). Typical Lux for daytime outside is greater than 10,000, while the ambient light of a typical night is less than 1 Lux [45].

Each of the three different sites used a different approach to remove the ambient sunlight. The first site was in a cave, which is naturally without sunlight. For the second site a black tarp was used to create a dark box for object scanning. The third and final site was in among the shallow areas of a sand bank island in the middle of the river. Due to having camp nearby, extra time at the site allowed for a preliminary visit to plan the scanning which would occur at night.

Section 4.4 RAHAS Capture Method

The procedure used to capture the RAHAS sequence is outlined in Figure 4.2. The first step was to position the system properly and to adjust the cameras so that the target object fills the field-of-view. The projector system was designed to be positioned a distance of 2 feet (within a few inches) from the target because the optics in the slide projector focused the pattern to this working distance. This required the placement of the prototype to be considered carefully when combined with environmental constraints such as deep water, ledges, and soft ground that could prevent the tripod's feet from making a sturdy base. The video camera and texture camera were optimally set when the target object spanned the complete width of the image frame. This allowed for the highest resolution 3-D scan of the object because more pixels of the image were used upon the object and not wasted on the background or areas that were not of interest. The scans that did not span the full width of the image frame were thrown out.

At the basis of the RAHAS capture sequence was the manual turning and sliding of the projected pattern using the projector prototype. The LED projector prototype is described in the previous chapter and Figure 3.2 shows the system with the controls

highlighted. The controls were manipulated to achieve motion of the pattern. During capture, attention was afforded to the projector, so that its time-on would be as little as possible so that the battery power could be conserved and the LED would not over heat. Also, since physical contact had to be made with the prototype to turn the mechanical assemblies, care had to be given to accidentally jarring the system. Bumping the system would cause an oscillation at the tripod mount and the video sequence would have a lateral jitter present, ruining the current scan data. As more scans were taken, the operator would steady his hand while using the system, which would result in better scans.

RAHAS Scanning Procedure

Reset the position of all the controls.

1. **Set Up RAHAS System –**
    a. Position 2 feet from *Target* – The projector is in-focus at this distance.
    b. Aim Cameras –Center *Target* in the Field of View of both cameras.
    c. Fix focus and zoom for both cameras – Camera focal length must be the same for calibration scan.
2. **RAHAS Sequence Capture –**
    a. Start video capture – Push the button on the video camera.
    b. Turn on projector – Being careful not to bump the system.
    c. Begin Rotation Sequence – Slowly move the lever maintaining a constant velocity.
    d. End Rotation Sequence – After lever reaches the limit stop.
    e. Begin Translation – Crank starts at 9 o'clock, carefully turn the crank clockwise.
    f. End Translation –When crank reaches 3 o'clock, stop.
    g. End Video Capture – Push the button again, being careful not to jar the system.
    h. Turn off projector.
    i. Capture Texture Image – Push button on center camera.
3. **Repeat RAHAS Sequence Capture on Calibration Grid.**

Figure 4.2 RAHAS Scanning Procedure. Outline of the process used for each scan performed in the field.

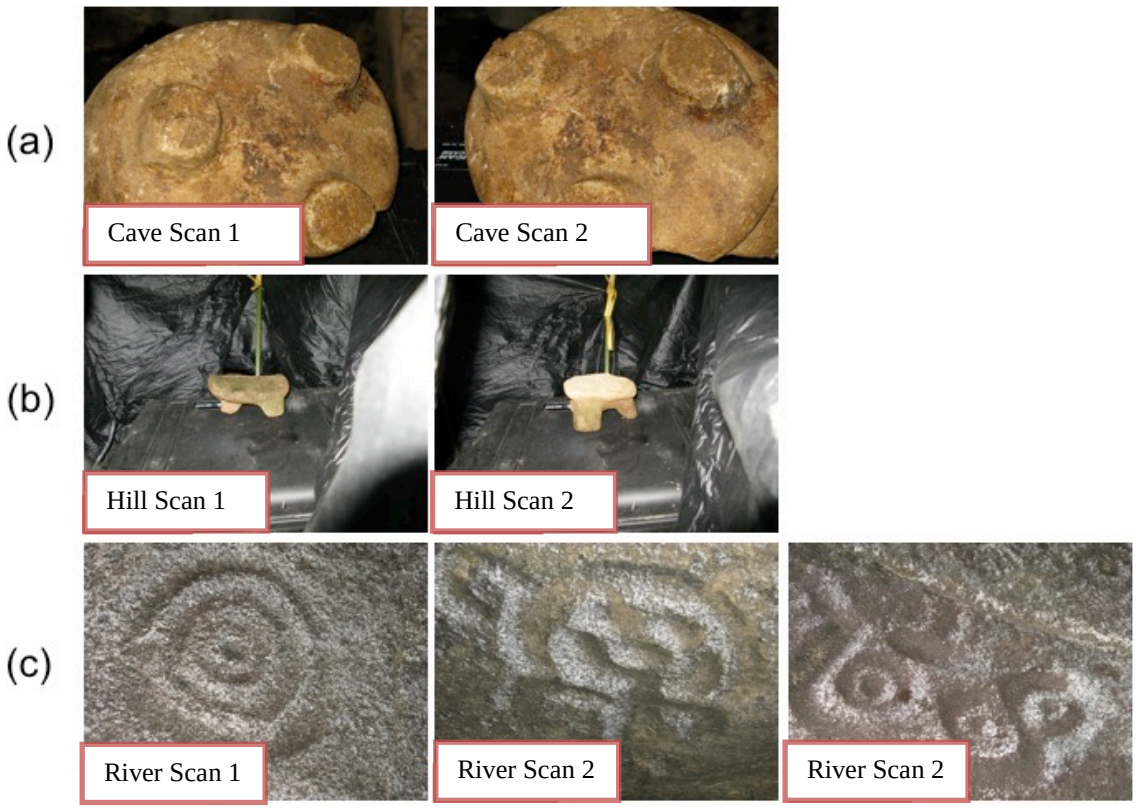

Figure 4.3 The seven objects to be scanned..a)Two views of a grinding stone from the first site (Cave) that was to be merged. b) The Hill Scans are not sufficiently large enough in the field of view. c) Petroglyphs on the rocks in the river that were taken at night.

Section 4.5 The Review of the Scans

In the field, a notebook was used to keep track of each scan's time, date, subject, and any comments related to the pattern motion sequence. After the expedition, this journal was used to both sort the scan data (video sequences and images) and as a resource to hasten the review of each scan. Each scan video sequence was viewed on a computer, and scans were thrown out if there were visible signs of system bounce or jarring in the video, or the object spanned less than half of the image width. The comments from the notebook helped with this process by including possible issues in each scan, such as whether the lever got stuck during rotation, if the projector system was bumped, or if the motion was smooth. It is important to note that the capture process occurs prior to processing and 3-

D generation, so a subjective quality measure of a scan sequence cannot be determined until viewed as a video. To combat the possibility of not returning with good usable data for this initial testing, redundant scans were taken when time allowed. These redundant scans were denoted in the field notebook.

In Figure 4.3, the objects scanned at each site are shown. The Cave Site (Fig. 4.3a) was thrown out because the projector system was jarred causing un-trackable motion. The scans from the hillside site, shown in Figure 4.3b, were thrown out due to poor object image span. From the images, the observed span of the object is close to 20% of the full number of pixels in the image.

Of the three sites, the third site was the only one that had scans that were actually processed. The increased quality of data at this last site is attributed to the experience gained during the previous scans, and the ample time spent at location allowing for both proper setup and redundant scans.

Figure 4.4 Final 3-D surface of the River Scan 2 (monkey petroglyph) after the mixed resolution texturing process.

Section 4.6 Presentation of RAHAS 3-D Data

The data collected at the final site in the shallows of the river is the focus of the3-D presentation, since the scans at the other sites were not processed. At the final site, the three scans were of petroglyphs, or rock carvings, and can be seen in Fig. 4.3c. While the symbolism of these carvings is unknown, these symbols can still be distinguished from each other based upon the pictorial content: the circle petroglyph (Scan 1), the monkey petroglyph (Scan 2), and the tri-circle petroglyph (Scan 3). The RAHAS 3-D reconstruction of the monkey petroglyph shown in Fig. 4.3c River Scan 2 produced the best result. The screen capture of the River Scan 2 (monkey) 3-D surface is shown in Figure 4.4.

A close-up view of the surface in Figure 4.4 is shown in Figure 4.5 so that the individual pixels denoting the world coordinates of the surface can be seen more easily. Each pixel has a color value that was captured using the texture image and combined using the mixed-resolution texture process (MxR). The scan resolution is shown, so the texture image was down-sampled to get the correct resolution.

Figure 4.5 The screen capture of the River Scan 2 surface zoomed. The three depressions of the surface in a triangular relationship can be seen in the middle of the face of the monkey petroglyph in Figure 4.4.

The surface shown in Fig. 4.4 and 4.5 was created from the wrapped phase and unwrapped phase images that are shown in Figure 4.6a and 4.6b respectively. Due to the use of the known snakes to unwrap the phase, the unwrapped phase cannot be generated for the regions of the image where the snakes are unknown. This is shown in the unwrapped phase image by the black regions of the image in Fig. 4.6b.

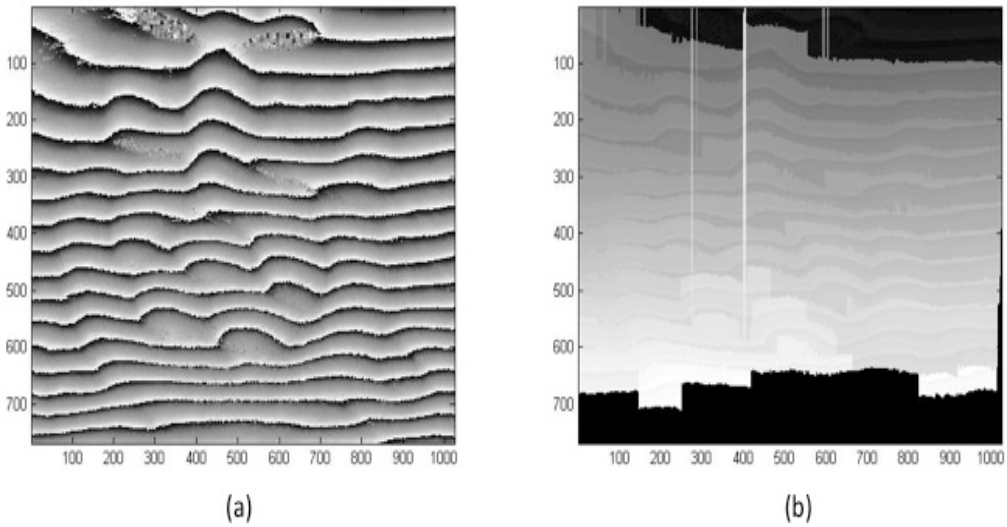

Figure 4.6 Phase images of River Scan 2. Shows (a) wrapped phase and (b) unwrapped phase.

It is important to note that the River Scan 2 (monkey petroglyph) shown in Fig. 4.4 has been corrected using a debandingprogramthatwas developed by Dr. Hassebrook.Theprocess involves the transformation to Projector Coordinate space for correction, and than back to Camera Coordinate space [55]. The uncorrected surface is shown in Figure 4.7a, and in Figure 4.7b with a side view to demonstrate the bands and striping phenomenon. The texture and quality images are shown in Figure 4.8; the grey and white stripes in the horizontal direction of Figure 4.8a are indicative of banding. Since the surface produced a continuous surface after the debanding process it is a minor occurrence of possible reconstruction artifacts. The comparison between this scan and those that follow will highlight how severe banding artifacts can cause the 3-D reconstruction process to be ineffectual at producing a surface that resembles the target.

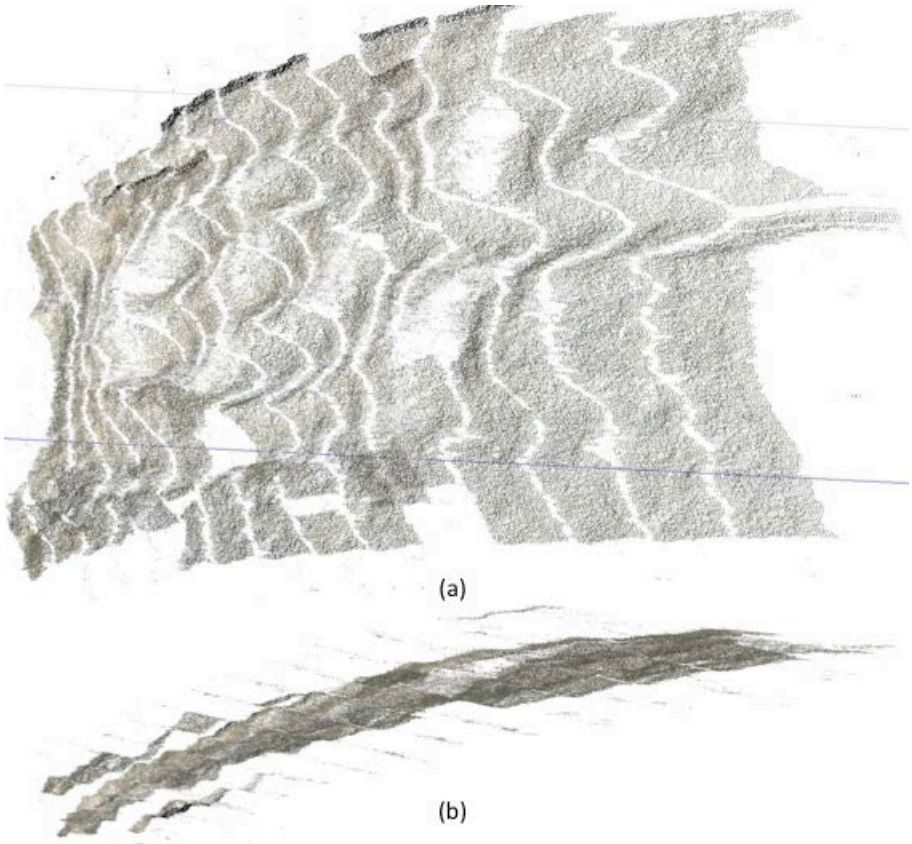

Figure 4.7 The uncorrected surface of the monkey petroglyph, River Scan 2. The perspective in (b) is a side view of (a) by a rotation of the surface.

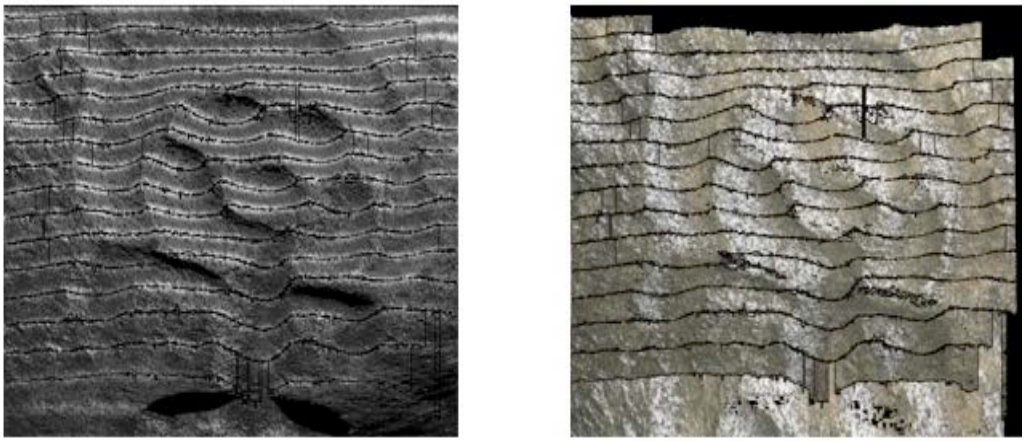

Figure 4.8 Shows both the (a) quality image of the River Scan 2, and (b) the texture image. Notice the black lines across each image which correspond to the regions near the boundaries of the Wrapped Phase.

The front view of the uncorrected concentric circle petroglyph of River Scan 1 is shown in Figure 4.9. On the far right side of the surface a vertical section was miss associated

with an incorrect phase value causing the section to track a trajectory not inline with the surface. This is shown in more detail in the side view of River Scan 1 in Figure 4.10.

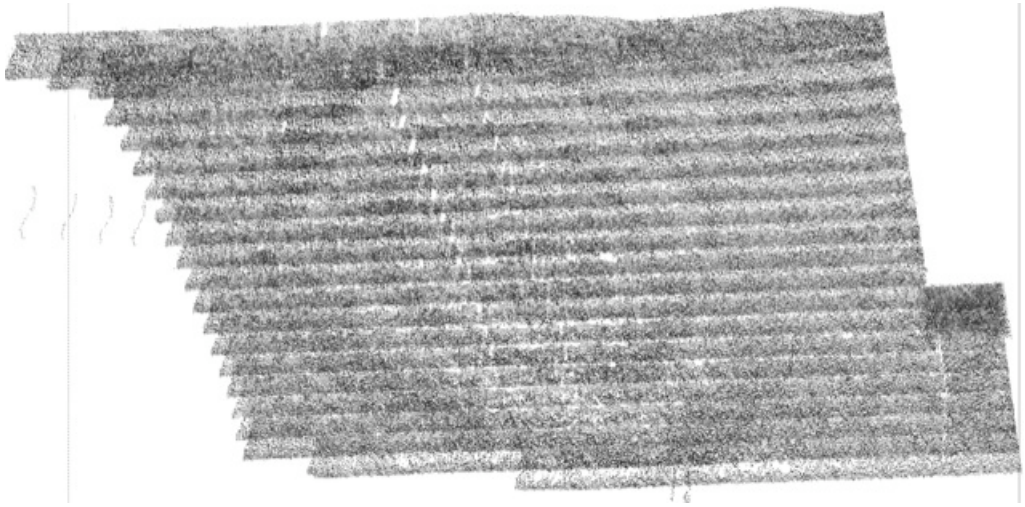

Figure 4.9 The uncorrected surface of the River Scan 1 circle petroglyph. This is an example of the reconstruction artifact called blinding.

The River Scan 1 is an example of the "window blinds," or "blinding" reconstruction artifact. "Blinding" is termed due to the wrapped phase bands being rotated 90 degrees from the correct surface orientation causing a similar looking pattern to the slated blinds of a window. The effect is exaggerated with the side perspective shown in Figure 4.10.

After correction, the "blinding" of River Scan 1 was removed, but an artifact still exists as roundness or curvature in the individual bands. Figure 4.11 shows the surface after correction.

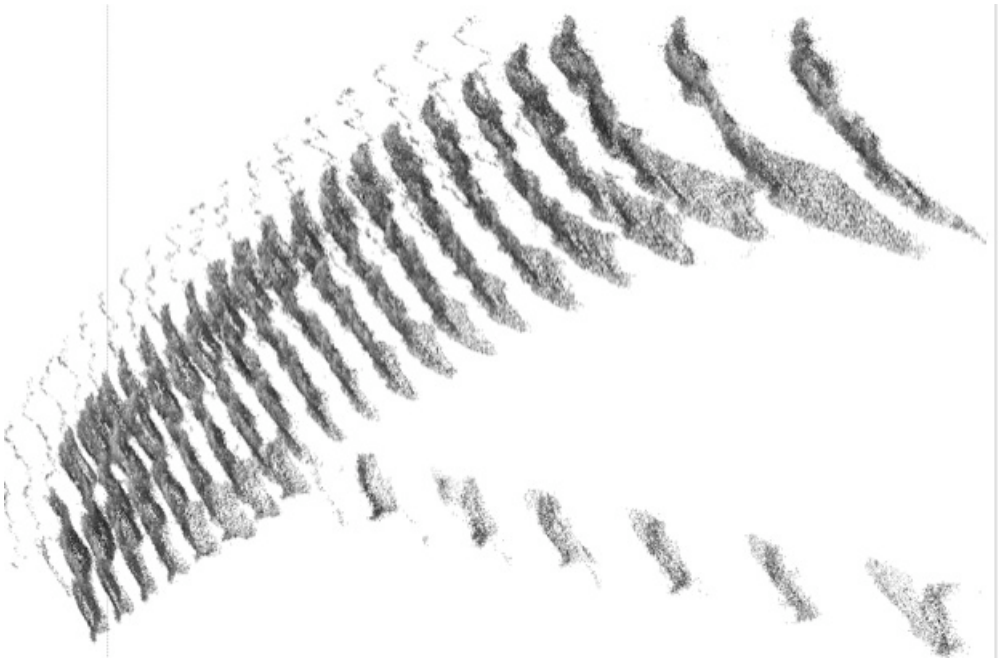

Figure 4.10 A rotated view of Figure 4.9, to look down the right side of the surface. This is to help in visualizing the window blind effect.

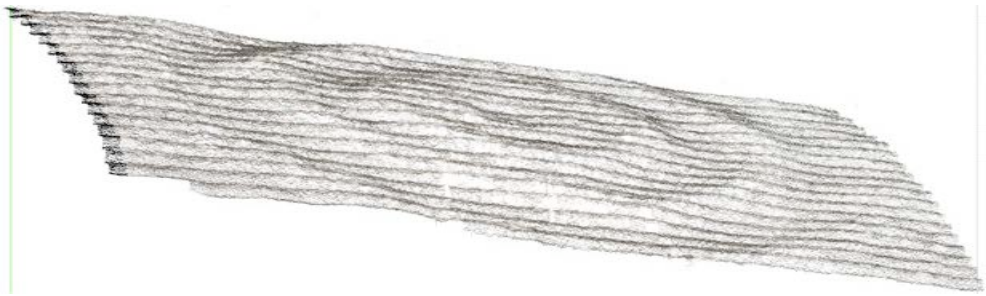

Figure 4.11 The corrected 3-D point cloud surface of the River Scan 1.

In Figure 4.12, the corrected River Scan 1 is rotated so the perspective is along the left side of the front view to present a profile of the bands. The curvature of the bands is in the phase direction of the pattern motion.

Figure 4.12 Side view of the River Scan 1 circle petroglyph for demonstrating the round contour of each band.

Shown in Figure 4.13 is the point cloud of the tri-circle petroglyph River Scan 3. The River Scan 3 had a problem that caused a step edge to occur at the boundaries of the Wrapped Phase.

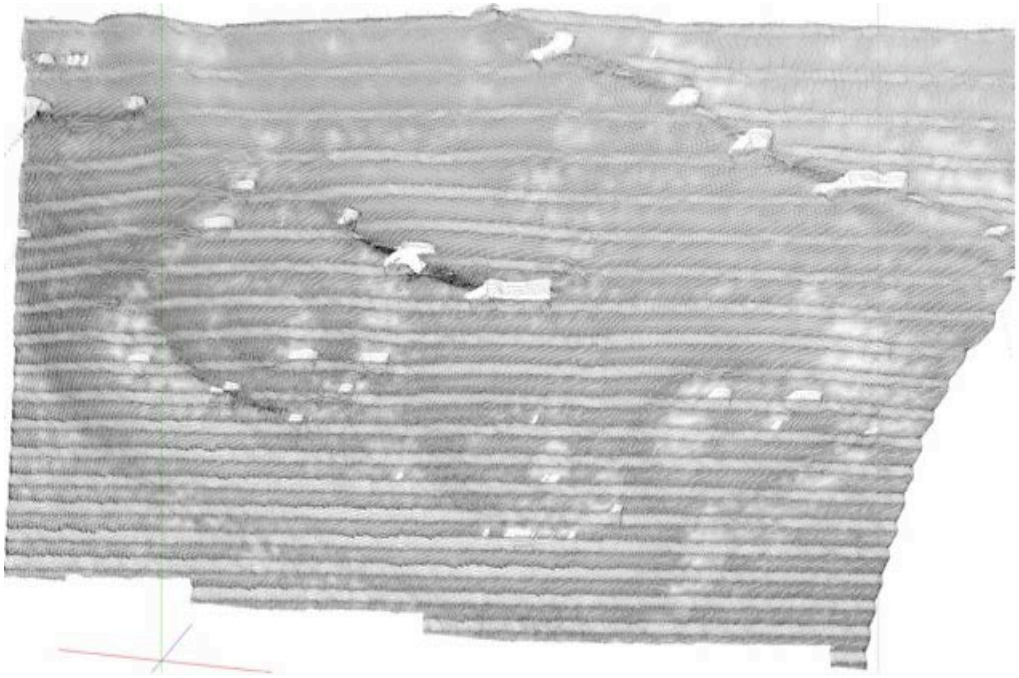

Figure 4.13 Surface point cloud showing the River Scan 3.

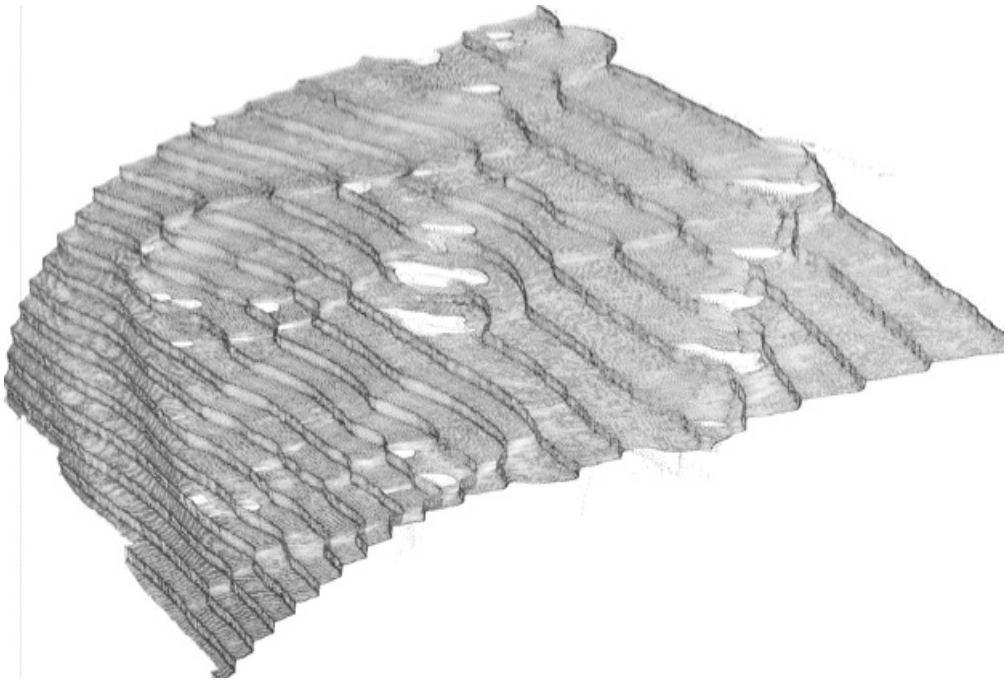

Figure 4.14 Rotated view of the surface of River Scan 3 to show the step edge banding effect.

The 3-D surface of River Scan 3 is shown rotated for easier viewing of the step edge in Figure 4.14. The same surface as that in Figure 4.14 is textured with the Quality Image, shown in Figure 4.15, to show the correlation between the black bands and the step edge.

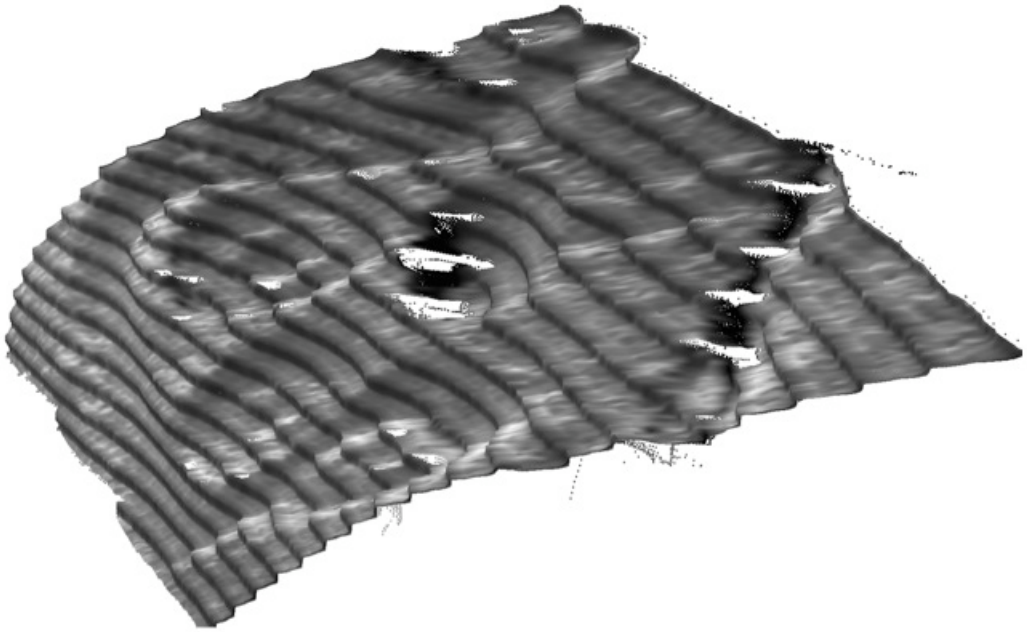

Figure 4.15 3-D Surface of River Scan 3. Same view as Figure 4.13, but with the Quality

image mapped to the surface to demonstrate the correlation of the black strip regions of the Quality image and the step edge.

Chapter 5
Conclusion and Future Work

This thesis introduced the RAHAS SLI technique for 3-D image acquisition, and shows the feasibility of a prototype scanner used as a measurement tool in a remote location. As part of the research, we built the prototype system, took the system to the jungles of Honduras to capture test data, and then brought the data back to the lab for processing. This scan data was used to develop an algorithm to generate 3-D images. This research shows that there is a way to measure and document material culture using 3-D Structured Light techniques in remote areas in the absence of generated power or a computer.

Section 5.1 Conclusions

We pushed the boundaries of SLI techniques by taking a scanner prototype to remote archaeological sites for field 3-D measurement, and learned valuable lessons related to the usage of RAHAS. First, a certain level of skill is critical to insure optimal data collection, since some of our data was compromised because I was not as practiced with the manual motion. Even though we tried to accommodate this with prior practice there was a clear progression of improvement from the first scans collected to the last scans. This improvement from first to last scans is also related to the amount of time spent at each site, with the time increasing from first to last. The way we overcame the user error in operation was to take multiple scans, but the expedition itinerary limited the amount of time that could be devoted to scanning at each site. Planning for enough time at each site is very important when traveling across the backcountry.

During the course of this research several factors affected the quality of the 3-D result. The snake tracking did not track every stripe perfectly throughout the rotation, however;

it turned out that it was not necessary to have perfect tracking through the rotation. The snakes could be identified in the first frame of the PMP translation and blank snakes filled in with a semi-manual process. Also of note is that when the PMP translation occurred the snakes identified in the first frame would be translated so that they were no longer in the image, and unlabeled snakes would enter the frame from the opposite side. This caused the field of 3-D rendering to diminish in area.

The most impactful issue was that the motion distortion of the temporal signals at each pixel, as a result of manual pattern translation, caused severe "banding" and other 3-D reconstruction artifacts. We present the concept of continuous-time sampling as a way to demonstrate the complexity associated with this issue, and with the hopes to determine a solution in the future.

Section 5.2 Future Work

When developing a new technology it can be difficult to determine when enough-is-enough, since research is a never-ending process; incremental improvements can always be made. The future of RAHAS and a few of the plans that we have for the RAHAS technique are now presented.

We know that the characterization of the motion distortion caused by the manual interface is the critical step in perfecting the RAHAS technique, and eliminating the need for skillful operation and streamlining the mechanical interface to slide motion. Perhaps allowing for the possibility of other 3-D scanners using manually motivated slides. We propose a concept for using snake motion to model the trajectory of motion, which is shown in Appendix A. The concept is an extension of the method used, but uses curve fitting of the trajectory of motion to interpolate values for the correct phase.

We plan on studying the use of the rotation of the pattern to encode each pixel with unique signals. The preliminary feasibility is demonstrated in Appendix C where it is

shown that there are specific signals generated at each pixel depending on the pixel's radius and angle from the center of pattern rotation. These specific signals are chirp-like, where a chirp signal is temporally compressed or expanded to achieve an increasing or decreasing frequency. The chirp could also be used to model the distortion characteristics used in RAHAS. The study of chirplets and the chirplet transform could be beneficial in further research and a group of papers devoted to the chirplet transform will be reviewed [46-48]. The chirplet transform is basically a wavelet transform that uses a mother wavelet shaped like a chirp signal [46], and is used to detect the presence of the frequency compression or expansion characteristic of specific chirp signals.

When dealing with prototypes, improvements to generated data can be made by refinement of the hardware. We plan on incorporating a motor assembly for constant motion of the slide pattern. Although as mentioned above, a more robust option could be to improve the modeling of motion and the associated corrective process. Ruggedizing the RAHAS hardware, and lightening the weight of a packed system further increases the practical use of the system in remote areas. Using a RAHAS 3-D scanner as a measurement tool in remote areas increases the hope of learning some new piece of information about past cultures and people.

Glossary: RAHAS Terminology

Active - A pixel is called an "active" snake pixel when it gets included into the Snake Matrix Set and has a non-zero value in the Si matrix. "active" implies that the pixel is also "valid"

Blank - Calling a pixel "blank" refers to its zero valued entry into the Si matrix.

Snake - A *snake* [RAR04,DH98] is a stripe of single pixel width that is located along the stripes of the sinusoidally varying pattern. For RAHAS processing, the *snake* identities are determined by SnakeFind functions and are stored in a Snake Matrix Set, which consist of three matrices {Si,Sy,Sp}.

Snake Matrix Set {Si, Sy, Sp} – A collection of three separate 2-D matrices that are used to identify and label snakes in a given image frame. The matrices are all the same size: the width is the width of the image, and the number of rows in the matrix corresponds to the number of snakes. Each entry in these matrices corresponds to a pixel on a snake, while a given row is a single snake. To index into a matrix, the x coordinate in the image is used along with the snake identity. For example, Sy(3,512) would return y coordinate of snake number 3 at the 512th column in the image.

Snake Identity Matrix, Si - The Si matrix is part of the Snake Matrix Set and is the indicator of whether a snake is valid or not. If a value of 0 is stored in the Si matrix, then the snake is not valid at that pixel. A value greater than 0 represents the identity given to the specific snake, and signifies an identified snake at the corresponding pixel. It is common to have snakes that do not span the whole width of the matrix, leaving gaps in the Si matrix to signify shadows on the object, undetected snake pixels, or that the stripe did not span the width of the image.

Snake Y Matrix, Sy - The Sy matrix is part of the Snake Matrix Set and holds the y-coordinate for the position of the corresponding snake pixel in the image. Since the snakes are oriented in the horizontal direction, the x values are used for indexing into the matrices

Snake Pixel Matrix, Sp - The Sp matrix is part of the Snake Matrix Set and holds the value of the pixel in the image that corresponds to that snake pixel.

Snake Mask, D - A trinary valued matrix the same size as an image in the capture sequence. D has the value 255 where the peaks of the snakes are located and a value of 128 transitioning between the peak locations and the rest of the image which is set to zero. The D image represents the pixels in the target image frame, A, that were identified as having peak characteristics of a snake. The D image is created by the function snakeMaskPeakPSR that will be outlined below.

Target Image, A - The target image *A* is the frame in the image sequence that is being processed. It will be denoted as *A*.

Valid- A pixel is called a "valid" snake pixel when it has a value of 255 in the Snake Mask D matrix. While a valid pixel will usually be active in the Si matrix, it could have been missed in the identification process and still be un-labeled.

Appendix A –
Sampling Concept and Motion Distortion for the RAHAS Scanning Interaction

As discussed in Section 3.3.1, the manual operation of the RAHAS prototype causes distortion, noticeable as a time-varying temporal compression and rarefaction of the expected sinusoidal signal at each pixel. The frictional and inertial forces that are in play against the crank rotation cause the initial speed to be slow and gradually build to a semi-constant rate with slight fluctuations. As a way to further elaborate on these concepts, two topics are presented: the modeling of the change in frequency by a concave upsweep quadratic chirp signal, and a curve fit to the trajectory of motion that the slide pattern undergoes.

The frequency of a chirp signal varies with time and is described by the second order equation

$$f(\tau) = f_0 + \beta\tau^2 \quad with \quad \beta = \frac{f_1 - f_0}{\tau_1} \quad and \quad f_1 > f_0 \tag{A.1}$$

where f_0 is the starting frequency or expected frequency of the sinusoidal signal, f_1 is the ending frequency at time τ_1. The time-domain signal of the quadratic upsweep chirp is determined by

$$x_c(t) = sin\,(2\pi \int_0^t f(\tau)d\tau) \tag{A.2}$$

with the integral for determining the instantaneous frequency of Equation A.1. The result of performing the integral in Equation A.2 on the frequency variation $f(\tau)$ of Equation A.1 is

$$x_c(t) = sin\left(2\pi\left(f_0 + \frac{\beta}{3}t^2\right)t\right) \tag{A.2}$$

where $x_c(t)$ represents the distorted signal at a pixel in continuous time t. Now, the discrete time sampling of a continuous system is applied to this chirp-based distortion model. A continuous time pulse train $s(t)$ in Equation A.3 is used to represent the video capture rate of the camera with sampling frequency of $1/T$, where T is the sampling interval.

$$s(t) = \sum_{-\infty}^{\infty} \delta(t - nT) \tag{A.3}$$

Using sampling theory, we get the Equation A.4 as the discrete time chirp signal, where k is the sample index, which is equivalent to nT.

$$x_s(k) = sin\left(2\pi\left(f_0 + \frac{\beta}{3}(k)^2\right)k\right) \tag{A.4}$$

The shape of the trajectory can be seen in Figure A.1.

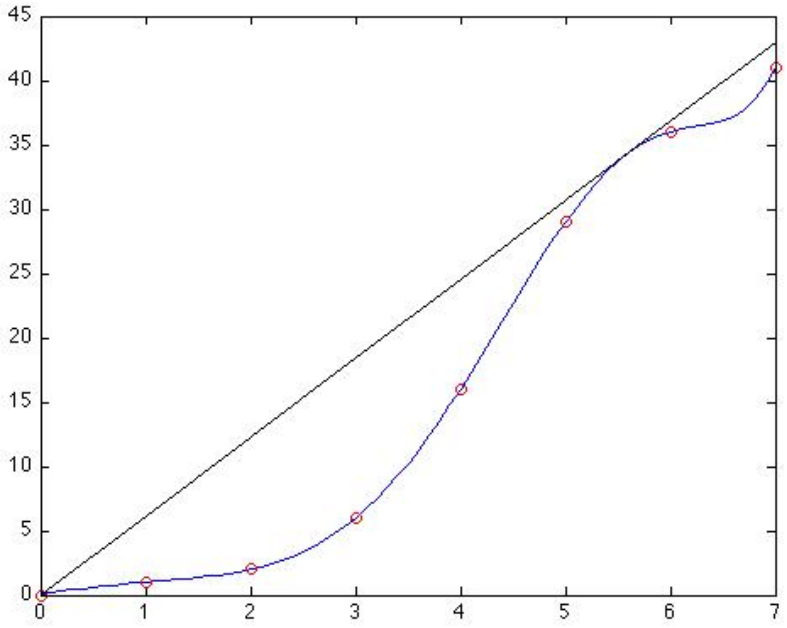

Figure A.1 Trajectory of motion for the manually translated pattern. The straight line signifies the ideal trajectory for uniform motion, while the curved line passing through the circles, represent the actual motion of the pattern.

Shown in Figure A.1, the position of the snake is represented by the red circles, with a best-fit curve connecting them. The diagonal line is the ideal uniform trajectory that we are trying to achieve. Using the known snake pixels of the stripes, the motion of the slide could be determined and corrected.

Appendix B –Rotation as a *Family* of Possibilities

The RAHAS technique uses the rotation of the pattern to "hold" onto the stripes in order to remove ambiguities of a high frequency PMP scan. While this is a simple method for unwrapping the phase, and appears to be a single variant of PMP, in reality, the RAHAS geometry opens up the possibility of rotation based encoding methods for projector-camera space mapping.

The image of a rotating sinusoidal pattern in projector space can be described by the equation

$$I_\theta^p(x^p, y^p) = A^p + B^p \cos\left(2\pi k_c \left(\sin(\theta)\frac{\left(y^p - y_0^p\right)}{M_y} + \cos(\theta)\frac{\left(x^p - x_0^p\right)}{N_x}\right)\right) \qquad \text{(B.1)}$$

where θ^p is the angle of clockwise rotation, k_c is the frequency of the sinusoidal pattern, (x_0^p, y_0^p) is the center of rotation, and (N_x, M_y) are the dimensions of the image.

In PMP, the linear translation of a sinusoidal pattern generates a sinusoidal signal at each pixel. Similarly, the rotation of a pattern will generate chirp shaped signals at each pixel whose characteristics are determined by the angle θ^p and radius r^p of the pixel from the center of pattern rotation.

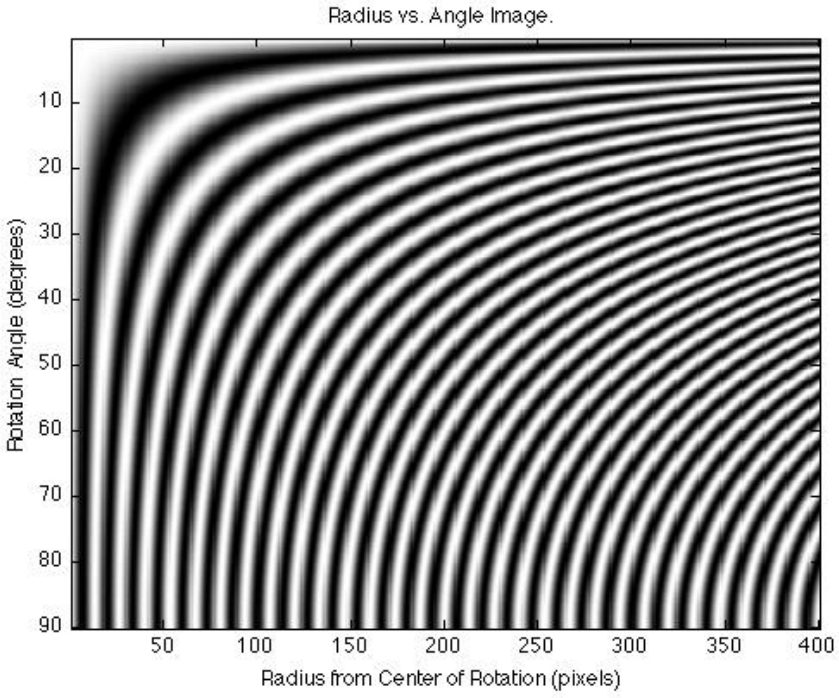

Figure B.1 Image of Radius vs. Rotation Angle. A comparison of the temporal signal at a pixel of a given radius vs. rotation angle from the center of rotation.

To further illustrate the characteristic patterns generated at each pixel, the Equation 2.2 for a PMP image in Cartesian coordinates (x^p, y^p) can be converted to polar coordinates (r^p, θ^p) as in the equation

$$I_n(r^p, \theta^p) = A(r^p, \theta^p) + B(r^p, \theta^p)\cos\left(2\pi k_c \frac{r^p \sin\left(\theta^p - \frac{\pi n}{2N_x}\right)}{M_y}\right) \quad \text{(B.2)}$$

wherer^p denotes the radius in the projector space, and θ^p is the rotation angle of the sinusoidal pattern. Using Equation B.2, an image $I_n(r^p, \theta^p)$ can be generated to display the relationship between pixel radius and angle, shown in Figure B.1.

A simulation of a rotated sinusoidal pattern was performed, so that signals at specific radii and angles could be observed. In Figure B.3, the angle of the test pixel is fixed to 30 degrees, and the radius is varied.

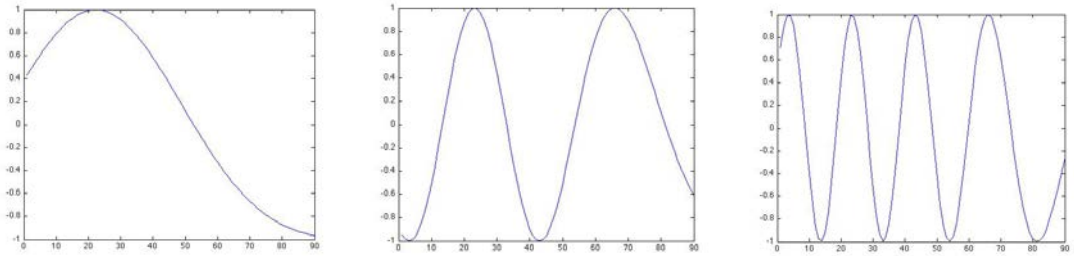

(a) (b) (c)

Figure B.2 Time-varying signal at pixels with a fixed angle, but varied radius. (a) radius 25, (b) radius 75, and (c) radius 150.

Now we look at how the signal changes when the radius is fixed at 100 pixels and the angle is varied. Notice that at 45 degrees B.3c, the signal looks sinusoidal or the chirp effect is minimized. This is because the pixels at 45 degrees are at a symmetric position relative to the 90 degree rotation of the pattern.

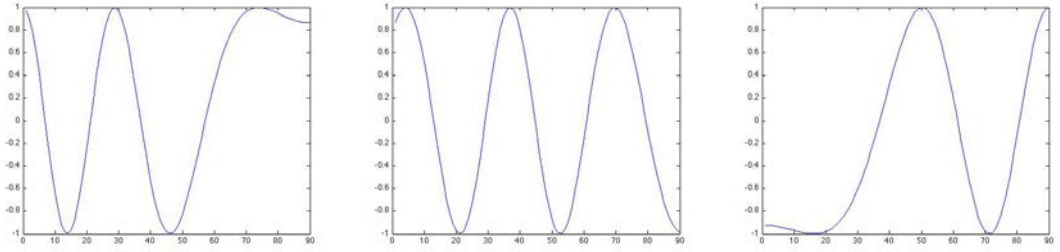

(a) (b) (c)

Figure B.3 Time-varying signal at pixels with a fixed radius, but varied angle. (a) angle of 0^o, (b) angle of 45^o, and (c) angle of 90^o.

References

[1] "shekel." Encyclopædia Britannica. 2010. Encyclopædia Britannica Online. 31 Oct. 2010 <http://www.britannica.com/EBchecked/topic/539589/shekel>.

[2] Stecchini, Livio C., A History of Measures. 2010. metrum.org 31 Oct. 2010 <http://www.metrum.org/measures/metrics.htm>

[3] Silverman, Joseph H..A Friendly Introduction to Number Theory, Prentice Hall, Third Edition 2006.

[4] "PantographiceseuArsdelineandi res quaslibet per parallelogrammumlineareseucavum" (Rome 1631).

[5] "pantograph." Encyclopædia Britannica. 2010. Encyclopædia Britannica Online. 31 Oct. 2010 <http://www.britannica.com/EBchecked/topic/441617/pantograph>.

[6] Weisstein, Eric W. "Pantograph." From MathWorld--A Wolfram Web Resource.<http://mathworld.wolfram.com/Pantograph.html>

[7] "History of the CMM," Web. 1 Nov. 2010. <http://www.cmmmetrology.co.uk/history_of_the_cmm.htm>

[8] K. Smith, "Coordinate Measuring Machines," Quality Digest, March 2002. Web 1 Nov. 2010. <http://www.qualitydigest.com/mar02/html/cmm.html> ,

[9] C. Bathow, M. Wachowiak."3D Scanning in Truly Remote Areas," CMSC, Charlotte, NC. 2008.

[10] S. D Cochran and G. Medioni, "3-D surface description from binocular stereo", *IEEE PAMI*, 14(10), pp. 981-994, 1992

[11] "Basics of Photogrammetry." Web. Feb. 2011. <www.geodetic.com/Downloadfiles/Basics of Photogrammetry.pdf>

[12] F. Chen, G. M. Brown, and M. Song, "Overview of three-dimensional shape measurement using optical methods," Opt. Eng. **39**, 10–22 (2000).

[13] X. Y. Su and W. S. Zhou, "Complex object profilometry and its application for dentistry," in *Clinical Applications of Modern Imaging Technology II*, L. J. Cerullo, K. S. Heiferman, Hong Liu, H. Podbielska, A. O. Wist, and L. J. Eamorano, eds., Proc. SPIE 2132, 484-489 (1994).Applications:

[14] G. Sansoni, F. Docchio, U. Minoni, and L. Biancardi, ''Adaptive profilometry for industrial applications,'' in Laser Applications to Mechanical Industry, S. Martellucci and A. N. Chester, eds. (Kluwer Academic, Norwell, Mass., 1993), pp. 351–365.

[15] D. Poussart and D. Laurendeau, “3-D sensing for industrial computer vision,” in *Advances in Machine Vision*, J. L. C. Sanz, ed. (Springer-Verlag, New York, 1989).

[16] Yongchang Wang, Qi Hao, AbhishikaFatehpuria, L. G. Hassebrook and D. L. Lau, “Quality and matching performance analysis of three-dimensional unraveled fingerprint,” *Optical Engineering*, Vol. **49**, No. 7, pp. 077202: 1-10, July (2010).

[17] G. Schmaltz of Schmaltz Brothers Laboratories, "A method for presenting the profile curvesof rough surfaces," Naturwiss 18, 315–316 (1932).

[18] Y. Shirai, M. Suwa, “Recognition of polyhedrons with a range finder,” in *Proceeding of the International Joint Conference on Artificial Intelligence* (Morgan Kaufman, San Francisco, Calif., 1971), pp. 80-87.

[19] J. L. Posdamer and M. D. Altschuler, “Surface measurement by space-encoded projected beam systems,” Comput. Vision Graph. Image Process. **18**, 1–17 (1982).

[20]P. M. Will, K. S. Pennington, “Grid coding: a preprocessing technique for robot and machine vision,” Artif. Intell. **2**, 319-329 (1971).

[21]K. Biderman, “Image encoding in modulated gratings from 1899-1970,” Opt.Acta 17, 631-635 (1970).

[22]D. M. Meados, W. O. Johnson, and J. B. Allen, “Generation of surface contours by moire patterns,” Appl. Opt. **9**, 942 (1970).Introduction to Three-Dimensional Acquisition

[23] K. L. Boyer and A. C. Kak, “Colored-encoded structured light for rapid active ranging,” IEEE Trans. Pattern Anal. Mach. Intell. 9, 14-28 (1987).

[24] C. Guan, “Composite Pattern for Single Frame 3D Acquisition”, *PhD Dissertation, University of Kentucky, Lexington*, USA, December 2004

[25]C. Guan, L. G. Hassebrook, D. L. Lau and V.G.Yalla, “Composite pattern structured light projection for human computer interaction in space,” spaceborne sensors II, SPIE’s Defense and security symposium 2005, Vol. 5798-05.

[26] C.Guan, L.G. Hassebrook and D.L. Lau, “Composite Structured light pattern for three dimensional video”, *Optics Express*, Vol. 11, Issue 5, pp. 406-417 (2003).

[27] R. C. Daley and L. G. Hassebrook, “Channel capacity model of binary encoded structured light stripe illumination,”AppliedOptics,Vol. 37, No. 17, (1998).

[28] H B Wu, Y Chen, M Y Wu, C R Guan and X Y Yu, “3D Measurement Technology by Structured Light Using Stripe-Edge-Based Gray Code”, Journal of Physics: Conference Series 48 (2006) 537–541doi:10.1088/1742-6596/48/1/101 International Symposium on Instrumentation Science and Technology.

[29] V. Srinivasan, H. C. Liu, and M. Halioua, "Automated phase-measuring profilometry of 3-D diffuse objects," Applied Optics, **23**, 3105-3108 (1984)

[30] Veera Ganesh Yalla , Laurence G. Hassebrook, " Very High resolution 3-D surface scanning Multi-Frequency Phase Measuring Profilometry" , spaceborne sensors II, SPIE's defense and Security symposium 2005, Vol. 5798-09.

[31] J. Li, L. G. Hassebrook, and C. Guan, "Optimized two-frequency phase-measuring profilometry light-sensor temporal-noise sensitivity," J. Opt. Soc. Am. A, 20(1), 2003.

[32] Veera Ganesh Yalla, Multi Frequency Phase Measuring Profilometry, *Masters Thesis*, University of Kentucky, Lexington, 2004

[33] Laurence G. Hassebrook, Aswinikumar Subramanian and PrashantPai, "Optimized three-dimensional recovery from two-dimensional images by means of sine wave structured light illumination", Optical Engineering 33(1), 219-229 (January 1994).

[34] G. Q. Wei, S. De Ma, "Implicit and explicit camera calibration: Theory and experiments", IEEE Trans. Pattern Anal. Mach. Intell. 16, pp. 469-480, 1994

[35] X. Armangue, J.Salvi, J, Batlle, "A comparative review of camera calibrating methods with accuracy evaluation", Pattern Recognition 35 (7) (2002) 1617--1635.

[36] L.G. Hassebrook, Notes on "Linear Triangulation surface reconstruction", 2-4-06.

[37]S. Zhang and P. S. Huang, "Novel Method for Structured Light System Calibration,"*Optical Engineering*, 2006.

[38] Sansoni, M. Carocci, R.Rodella, " Calibration and performance evaluation of a 3D imaging sensor based on the projection of structured light", IEEE Trans. Instrumentation and Measurement, 49(3), 628-636, 2000

[39] L G Hassebrook, UK Scanner Calibration, Nov. 2009. Web. Nov. 2010. <www.engr.uky.edu/~lgh/soft/softscannercalibration.htm>

[40] L. G. Haseebrook, D. L. Lau, "Structured Light Illumination Strategy: Introduction of Lock and Hold Structured Light Illumination," University of Kentucky EE Report #CSP 06-004, 2-20-06, Revised 5-26-06

[41] C.J. Casey, "Structured Light Motion Capture," M.S. Thesis, University of Kentucky, Lexington, KY, USA, 2008

[42] A. Robinson, L. Alboul, and M. Rodrigues. "Methods for indexing stripes in uncoded structured light scanning systems," *Journal of WSCG*, 12(3):371-378, February 2004

[43] R. B. Fisher, D. K. Naidu, "A Comparison of Algorithms for Subpixel Peak Detection," *Advances in Image Processing, Multimedia and Machine Vision*, Springer-Verlag, Heidelberg, 1996

[44] L. G. Hassebrook, C. J. Casey and W. F. Lundby, "Non-Contact Fiducial Based 3-Dimensional Patch Merging Methodology and Performanc," Proceedings of the 2009 Computer Applications and Quantitative Methods in Archaeology Conference, Williamsburg, VA, March 2009

[45] W. L. Long, "Illuminance." 1992. Web. Feb. 2011. <www.drdrbill.com/downloads/optics/photometry/Illuminance.pdf>.

[46] S. Mann, S. Haykin, "Adaptive "chirplet" transform: an adaptive generalization of the wavelet transform," Optical Engineering 31(6), 1243- 1256 (June 1992).

[47] S. Mann, S. Haykin, "The adaptive chirplet: an adaptive generalized wavelet—like transform," SPIE Vol. 1565 Adaptive Signal Processing, 402-413 (1991)

[48] R. Ashino, M. Nagase, R. Vaillancourt, "Gabor, wavelet and chirplet transforms in the study of pseudodifferential operators," CRM-2528, January 1998.

[49] J. K. Aggarwal and Y. F. Wang, "Inference of object surface structure from structured lighting – an overview," in *Machine Vision*, Herbert Freeman, ed. (Academic, Boston, 1988), pp. 193-220.

[50] G. Sansoni, F. Docchio, U. Minoni, and L. Biancardi, ''Adaptive profilometry for industrial applications,'' in *Laser Applications to Mechanical Industry*, S. Martellucci and A. N. Chester, eds. (Kluwer Academic, Norwell, Mass., 1993), pp. 351–365.

[51] D. S. Goodman and L. G. Hassebrook, "Face recognition under varying pose," IBM Technical Disclosure Bulletin **27**, 2671–2673 (1984).

[52] B. Carrihill and R. Hummel, "Experiments with intensity ratio depth sensor," Comput.VisionGraph. Image Process. **32**, 337–358 (1985).

[53] M. Maruyama and S. Abe, "Range sensing by projecting multiple slits with random cuts," IEEE Trans. Pattern. Anal. Mach. Intell. **15**, 647–651 (1993).

[54] G. Goli, C. Guan, L. G. Hassebrook, and D. L. Lau, "Video rate three dimensional data acquisition using composite light structure pattern," Tech. Rep. CSP 02-002, University of Kentucky, Department of Electrical and Computer Engineering, Lexington, KY USA (2002).

[55] A. G. Pethe, "Super Resolution 3D Scanning," *M. S. Thesis*, University of Kentucky, Lexington, KY, 2008.

Vita

Author's Name Eli Ross Crane

Birth Place Lexington, KY, USA
Birth Date May 9, 1979

Education Bachelor of Science in Electrical Engineering
University of Kentucky, 2004

Publications

C. J. Casey, L. G. Hassebrook, E. R. Crane, A. Davidson, "Multi-Feature Distortion-Insensitive Constellation Detection," *Applied Optics,* Accepted 2011.

E. R. Crane, L.G. Hassebrook, C.T. Begley, W. F. Lundby and C. J. Casey, "Methodology and Technology for Rapid Three-Dimensional Scanning of In Situ Archaeological Materials in Remote Areas," Edited by Bernard Breuckmann. Presented in Interpretation and Evaluation of High Definition 3D Surface Data III. *Computer Applications and Quantitative Methods in Archaelogy*, Granada, Spain (April 2010).

K. D. Donohue, D. C. Medonza, E. R. Crane and B. F. O'Hara, "Assessment of a non-invasive high-throughput classifier for behaviours associated with sleep and wake in mice," *BioMedical Engineering OnLine*, 7:14 (11 Apr 2008)

Provisional Patent

L.G. Hassebrook, Charles J. Casey, Eli R. Crane, Walter F. Lundby, Kai Liu, Yongchang Wang, and Daniel L. Lau, "Rotate and Hold and Scan (RAHAS) Structured Light Illumination Pattern Encoding and Decoding," Filed 6/24/2010. Application No. 61/358,397, UKRF-136P.